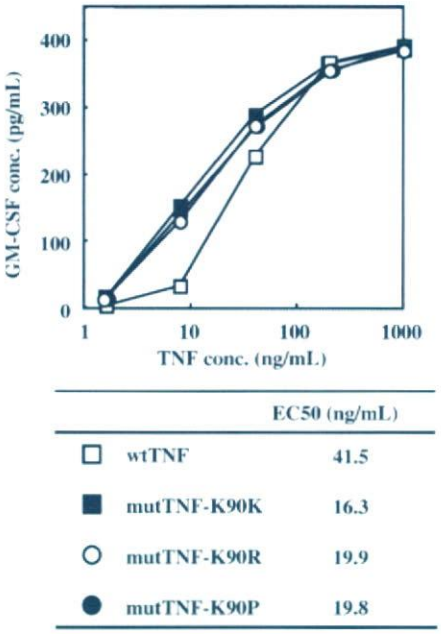

Fig. 6. Induction of GM-CSF by mutTNFs. PC60 cells transfected human TNFR2 were incubated with mutTNFs and IL-1β (2 ng/mL). After 24 h, TNFR2-mediated induction of GM-CSF was assayed by ELISA. Each value represents the mean±SD. The EC_{50} is given as the concentration of TNF-α required to induce secretion of 200 pg/mL GM-CSF.

lower bioactivity of mutTNF-R90P via TNFR1 may be due to weaker affinity for TNFR1. On the other hand, affinities of the three mutTNFs for TNFR2 were 1.2- to 1.5-fold higher than that of wtTNF (Table 2). These results suggest that replacement of amino acid residue 90 in mutTNF does not affect the affinity for TNFR2, while arginine or lysine substitution at amino acid residue 90 is better than proline for TNFR1 binding.

4. Discussion

Although systemic administration of TNF-α is limited due to its severe side effects, TNF exerts beneficial anti-tumor effects as an enhancer of tumor vascular permeability in combination cancer chemotherapy [8–10]. Therefore, the creation of an artificial mutTNF with remarkable bioactivity and in vivo

Table 1
Kinetic parameters of mutant TNF-αs (TNF receptor 1)

	Ka[a] (10^5)(1/Ms)	Kd[b] (10^{-3})(1/s)	KD[c] (10^{-9})(M)	Relative[d] (%)
Human wtTNF	5.4	1.2	2.3	100
mutTNF-R90K	13.4	1.1	0.8	285
mutTNF-R90P	4.0	2.1	5.2	44
mutTNF-R90R	12.1	1.4	1.2	191

Kinetic parameters were determined from equilibrium binding using BIA evaluation 3.0 program.

[a] Association rate constant.

[b] Dissociation rate constant.

[c] Equilibrium dissociation constant.

[d] Relative values for the KD were calculated from the KD (mutants)/KD (wtTNF)×100.

Table 2
Kinetic parameters of mutant TNF-αs (TNF receptor 2)

	Ka[a] (10^6) (1/Ms)	Kd[b] (10^{-4}) (1/s)	KD[c] (10^{-10}) (M)	Relative[d] (%)
Human wtTNF	3.7	10.1	2.7	100
mutTNF-R90K	5.1	10.7	2.1	129
mutTNF-R90P	5.1	11.3	2.2	122
mutTNF-R90R	5.2	9.4	1.8	148

Kinetic parameters were determined from equilibrium binding using BIA evaluation 3.0 program.

[a] Association rate constant.

[b] Dissociation rate constant.

[c] Equilibrium dissociation constant.

[d] Relative values for the KD were calculated from the KD (mutants)/KD (wtTNF)×100.

stability will be important to generate a more effective cancer chemotherapy. We have previously created lysine-deficient mutTNFs, mutTNF-R90 and P90, which showed high bioactivity and in vivo stability and are suitable for site-specific mono-PEGylation [18]. We have also reported that these lysine-deficient mutTNFs show the same or higher bioactivities than wtTNF and that mono-PEGylated mutTNFs exhibit increased anti-tumor therapeutic potential. In this study, we attempted to create a new mutTNF that has more bioactivity and a tighter binding affinity when compared to mutTNF-R90 and P90. We also evaluated the role of amino acid residue 90 in bioactivity and receptor binding capacity.

We constructed a phage library that expresses mutTNF-R90 variants in which R90 is replaced with other amino acids and measured their affinities for anti-TNF-α and their bioactivities using culture supernatant of *E. coli*. Only mutTNF-R90X in which amino acid residue 90 was replaced with lysine, arginine, or proline exhibited affinity for anti-TNF-α and bioactivity. Therefore, it is suggested that proline, arginine and lysine at position 90 are important to retain the bioactivity of TNF-α. As described previously, K90 in wtTNF forms a hydrogen bond with E135 in TNFR1 and contributes to stabilizing the loop structure that contains residues 84 to 89, which is the receptor binding region. In the mutTNF-R90R, R90 also likely forms a hydrogen bond with E135 and perhaps contributes to stabilizing the loop structure. The basic amino acid substitution mutTNF-R90H had no bioactivity nor binding affinity. These results suggest that general replacement of R90 with a basic amino acid is not always essential for bioactivity and binding affinity to the TNF receptor. Moreover, the steric hindrance of an amino acid residue is as important as electric charge.

Lysine residues in proteins are generally believed to be important amino acids for retaining three-dimensional structure and for receptor affinity and bioactivity. In the case of TNF-α, X-ray structure analysis revealed that K11 and K98 are important for retaining protein structure and homotrimerization [20]. However, the importance of other lysine residues (K65, 90, 112, 128) has not been discussed. The only report with regard to K90 demonstrated that replacement of K90 with alanine reduced the bioactivity to half of wtTNF [21]. Our results indicate that amino acid position 90 of TNF-α is important for homotrimer formation and bioactivity.

We measured the bioactivities and affinities of mutTNF-R90R, R90K and R90P for TNF receptors. mutTNF-R90R and mutTNF-R90K demonstrated 10-fold higher cytotoxicity levels in HEp-2 cells than wtTNF. The cytotoxicity level of mutTNF-R90P was almost the same as wtTNF. Indeed, affinities of mutTNF-R90R and -R90K for TNFR1 were 2 to 3-fold higher than wtTNF, while that of mutTNF-R90P was half that of wtTNF. Thus R90 and K90 contribute to the stable formation of the TNF/TNFR1 complex, and this may be one of the factors causing increased bioactivity. On the other hand, TNFR2-dependent bioactivities of the three mutants almost doubled that of wtTNF. Affinities of the three mutants for TNFR2 were also 1.2 to 1.5 stronger that that of wtTNF. These results indicate that arginine or lysine in amino acid position 90 is necessary for mutTNFs to obtain superior bioactivity and affinity for TNFR1, but less so for TNFR2. A previous study showed that the loop structure mutant TNF S86T had TNFR1-selectivity [22]. The interaction site of this loop structure with TNFR1 is predicted to be different than with TNFR2. The lower affinity of mutTNF-R90P for TNFR1 (as compared with mutTNF-R90K or-R90R) is thought to be caused by the difference in loop structure stabilization. The hydrogen bond formed between the basic amino acid (K90 or R90) and E135 creates a more stable loop than one stabilized by the hydrophobic bond between P90 and L83. Interestingly, in the lysine-deficient mutTNF that we previously created, K90 was replaced with proline [19]. This result indicates that the loop structure formed by the hydrophobic interaction of P90 with L83 is very important to protein folding and homotrimer formation.

In this study, we created mutTNFs that substitute other amino acids in the K90 position and evaluated their bioactivities and binding affinities. The determination of the functional domain of TNF has been attempted by creating mutant TNFs like these, however, there are few reports that detailed the role of one amino acid in TNF-α. Our data demonstrate that amino acid position 90 is important for TNF bioactivity and that replacement with other amino acids will be an effective strategy to increase the bioactivity of TNF-α. In the near future, the accumulation of information about the structure–activity relationship of TNF-α using mutant TNFs will enable the generation of a super-agonist that has optimized bioactivity.

Acknowledgements

This study was supported by a Grant-in-Aid for Scientific Research (No. 17016084 and 17689008, 17790135, 18015055, 18659047) from the Ministry of Education, Culture, Sports, Science and Technology of Japan, a Health and Labor Sciences Research Grant from the Ministry of Health, Labor and Welfare of Japan, Takeda Scientific Foundation and Research Fellowships for Young Scientists.

References

[1] E.A. Carswell, L.J. Old, R.L. Kassel, S. Green, N. Fiore, B. Williamson, An endotoxin-induced serum factor that causes necrosis of tumors, Proc. Natl. Acad. Sci. U. S. A. 72 (1975) 3666–3670.

[2] E.A. Havell, W. Fiers, R.J. North, The antitumor function of tumor necrosis factor (TNF), I. Therapeutic action of TNF against an established murine sarcoma is indirect, immunologically dependent, and limited by severe toxicity, J. Exp. Med. 167 (1988) 1067–1085.

[3] L. Helson, C. Helson, S. Green, Effects of murine tumor necrosis factor on heterotransplanted human tumors, Exp. Cell Biol. 47 (1979) 53–60.

[4] W.L. Furman, D. Strother, K. McClain, B. Bell, B. Leventhal, C.B. Pratt, Phase I clinical trial of recombinant human tumor necrosis factor in children with refractory solid tumors: a Pediatric Oncology Group study, J. Clin. Oncol. 11 (1993) 2205–2210.

[5] K. Kimura, T. Taguchi, I. Urushizaki, R. Ohno, O. Abe, H. Furue, T. Hattori, H. Ichihashi, K. Inoguchi, H. Majima, Phase I study of recombinant human tumor necrosis factor, Cancer Chemother. Pharmacol. 20 (1987) 223–239.

[6] T. Moritz, N. Niederle, J. Baumann, D. May, E. Kurschel, R. Osieka, J. Kempeni, E. Schlick, C.G. Schmidt, Phase I study of recombinant human tumor necrosis factor alpha in advanced malignant disease, Cancer Immunol. Immunother. 29 (1989) 144–150.

[7] J. Skillings, R. Wierzbicki, E. Eisenhauer, P. Venner, F. Letendre, D. Stewart, B. Weinerman, A phase II study of recombinant tumor necrosis factor in renal cell carcinoma: a study of the National Cancer Institute of Canada Clinical Trials Group, J. Immunother. 11 (1992) 67–70.

[8] A.M. Eggermont, H. Schraffordt Koops, D. Lienard, B.B. Kroon, A.N. van Geel, H.J. Hoekstra, F.J. Lejeune, Isolated limb perfusion with high-dose tumor necrosis factor-alpha in combination with interferon-gamma and melphalan for nonresectable extremity soft tissue sarcomas: a multicenter trial, J. Clin. Oncol. 14 (1996) 2653–2665.

[9] D. Lienard, P. Ewalenko, J.J. Delmotte, N. Renard, F.J. Lejeune, High-dose recombinant tumor necrosis factor alpha in combination with interferon gamma and melphalan in isolation perfusion of the limbs for melanoma and sarcoma, J. Clin. Oncol. 10 (1992) 52–60.

[10] F.J. Lejeune, Clinical use of TNF revisited: improving penetration of anti-cancer agents by increasing vascular permeability, J. Clin. Invest. 110 (2002) 433–435.

[11] F.J. Lejeune, C. Ruegg, D. Lienard, Clinical applications of TNF-alpha in cancer, Curr. Opin. Immunol. 10 (1998) 573–580.

[12] P. Bailon, A. Palleroni, C.A. Schaffer, C.L. Spence, W.J. Fung, J.E. Porter, G.K. Ehrlich, W. Pan, Z.X. Xu, M.W. Modi, A. Farid, W. Berthold, M. Graves, Rational design of a potent, long-lasting form of interferon: a 40 kDa branched polyethylene glycol-conjugated interferon alpha-2a for the treatment of hepatitis C, Bioconjug. Chem. 12 (2001) 195–202.

[13] H. Kamada, Y. Tsutsumi, K. Sato-Kamada, Y. Yamamoto, Y. Yoshioka, T. Okamoto, S. Nakagawa, S. Nagata, T. Mayumi, Synthesis of a poly (vinylpyrrolidone-co-dimethyl maleic anhydride) co-polymer and its application for renal drug targeting, Nat. Biotechnol. 21 (2003) 399–404.

[14] H. Kamada, Y. Tsutsumi, Y. Yamamoto, T. Kihira, Y. Kaneda, Y. Mu, H. Kodaira, S.I. Tsunoda, S. Nakagawa, T. Mayumi, Antitumor activity of tumor necrosis factor-alpha conjugated with polyvinylpyrrolidone on solid tumors in mice, Cancer Res. 60 (2000) 6416–6420.

[15] Y. Kaneda, Y. Yamamoto, H. Kamada, S. Tsunoda, Y. Tsutsumi, T. Hirano, T. Mayumi, Antitumor activity of tumor necrosis factor alpha conjugated with divinyl ether and maleic anhydride copolymer on solid tumors in mice, Cancer Res. 58 (1998) 290–295.

[16] Y. Tsutsumi, S. Tsunoda, H. Kamada, T. Kihira, Y. Kaneda, Y. Ohsugi, T. Mayumi, PEGylation of interleukin-6 effectively increases its thrombopoietic potency, Thromb. Haemost. 77 (1997) 168–173.

[17] S.P. Monkarsh, Y. Ma, A. Aglione, P. Bailon, D. Ciolek, B. DeBarbieri, M.C. Graves, K. Hollfelder, H. Michel, A. Palleroni, J.E. Porter, E. Russoman, S. Roy, Y.C. Pan, Positional isomers of monopegylated interferon alpha-2a: isolation, characterization, and biological activity, Anal. Biochem. 247 (1997) 434–440.

[18] H. Shibata, Y. Yoshioka, S. Ikemizu, K. Kobayashi, Y. Yamamoto, Y. Mukai, T. Okamoto, M. Taniai, M. Kawamura, Y. Abe, S. Nakagawa, T. Hayakawa, S. Nagata, Y. Yamagata, T. Mayumi, H. Kamada, Y. Tsutsumi, Functionalization of tumor necrosis factor-alpha using phage display technique and PEGylation improves its antitumor therapeutic window, Clin. Cancer Res. 10 (2004) 8293–8300.

[19] Y. Yamamoto, Y. Tsutsumi, Y. Yoshioka, T. Nishibata, K. Kobayashi, T.

Okamoto, Y. Mukai, T. Shimizu, S. Nakagawa, S. Nagata, T. Mayumi, Site-specific PEGylation of a lysine-deficient TNF-alpha with full bioactivity, Nat. Biotechnol. 21 (2003) 546–552.
[20] M.J. Eck, S.R. Sprang, The structure of tumor necrosis factor-alpha at 2.6 A resolution. Implications for receptor binding, J. Biol. Chem. 264 (1989) 17595–17605.
[21] J. Yamagishi, H. Kawashima, N. Matsuo, M. Ohue, M. Yamayoshi, T. Fukui, H. Kotani, R. Furuta, K. Nakano, M. Yamada, Mutational analysis of structure–activity relationships in human tumor necrosis factor-alpha, Protein Eng. 3 (1990) 713–719.
[22] H. Loetscher, D. Stueber, D. Banner, F. Mackay, W. Lesslauer, Human tumor necrosis factor alpha (TNF alpha) mutants with exclusive specificity for the 55-kDa or 75-kDa TNF receptors, J. Biol. Chem. 268 (1993) 26350–26357.

Department of Biopharmaceutics[1], Graduate School of Pharmaceutical Sciences, Osaka University, Laboratory of Pharmaceutical Proteomics (LPP)[2], National Institute of Biomedical Innovation (NiBio), Frontier Research Center[3], Osaka University (FRC), Osaka, Japan

Creation of a novel cell penetrating peptide, using a random 18mer peptides library

T. Nomura[1,2], M. Kawamura[1], H. Shibata[1,2,3], Y. Abe[1,2], A. Ohkawa[1,2], Y. Mukai[1,2], T. Sugita[1,2], S. Imai[1,2], K. Nagano[1,2], T. Okamoto[1], Y. Tsutsumi[1,2], H. Kamada[2], S. Nakagawa[1,3], S. Tsunoda[2]

Received December 1, 2006, accepted December 18, 2006

Haruhiko Kamada, Ph.D, Laboratory of Pharmaceutical Proteomics, National Institute of Biomedical Innovation (NiBio), 7-6-8 Saito-Asagi, Ibaraki, Osaka 567-0085, Japan
kamada@nibio.go.jp

Pharmazie 62: 569–573 (2007) *doi: 10.1691/ph.2007.8.6278*

Cell penetrating peptides (CPPs) have drawn attention as carriers for intracellular drug delivery. It is commonly believed that TAT peptide is the best carrier among the existing CPPs due to its high translocational activity. Despite considerable research, the cellular uptake mechanism of TAT peptide remains unclear. Additionally, the transduction efficiency of TAT peptide is insufficient for use in intracellular therapy. In this study, we attempted to identify novel CPPs from a random 18mer peptide library using a phage display system. To isolate novel CPPs more effectively, PSIF (protein synthesis inhibition factor) was used with the screening system. Consequently, we isolated 7 novel CPPs from the library and determined by flow cytometry and confocal laser microscopy that these CPPs were taken up into cells. Once the cellular uptake pathway of these CPPs has been determined, it may be possible to use them for intracellular therapy.

1. Introduction

With the progress of proteomics technology over the last few years, many disease-related proteins have been discovered (Kuncl et al. 2002; Lambrechts et al. 2003; St Croix et al. 2000). Many of these proteins reside within the cell. To therapeutically modulate disease-related-proteins, effective methods are needed to deliver other regulatory proteins into cells. Recently, cell penetrating peptides (CPPs) have received considerable attention in this regard (Derossi et al. 1998; Wadia and Dowdy 2002). Examples of CPPs include short peptide segments derived from HIV-1 TAT (Frankel and Pabo 1988; Green and Loewenstein 1988) (13 a.a), *Drosophila* Antennapedia homeodomain proteins (Joliot et al. 1991) (16 a.a), and *Herpes simplex* virus VP22 (Elliott and O'Hare 1997) (17 a.a) are examples of CPP peptides. Because CPPs can translocate various molecules (e.g., peptides, proteins, plasmids, and nucleotides (Astriab-Fisher et al. 2000)) into the cells, CPPs are expected to be useful as carriers for intracellular drug delivery. Of the existing CPPs, TAT peptide is the most effective carrier, and has been used as a carrier to deliver p53 protein for tumor suppression (Li et al. 2002). There are several factors, however, that limit the therapeutic use of CPPs. Firstly, although the mechanism of translocation is thought to be mediated via an endocytic pathway, the precise mechanism of how TAT peptide translocates across the membrane and escapes from the endosome remains unclear. Secondly, the transduction efficiency of TAT peptide is too low to effectively modulate disease-related-proteins. Therefore, for intracellular therapy, novel CPPs are needed that can introduce target proteins into cells more efficiently than existing CPPs by different mechanisms.

Phage libraries expressing polypeptides, such as single-chain antibodies (Imai et al. 2006; Okamoto et al. 2004) or random peptides (Chung et al. 2002; Connor et al. 2001; Scott and Smith 1990), have been used extensively to identify specific molecules with high affinity for target ligands. In the past, novel CPPs have been developed using random peptide phage libraries and cell panning (Hou et al. 2004; Landon and Deutscher 2003; Mi et al. 2003). However, with cell panning, cell-penetrating peptides are difficult to obtain because these peptides bind to the entire cell surface. We previously developed an effective system for screening CPPs using PSIF (protein synthesis inhibition factor). PSIF, a bacteria-derived protein toxin, is non-cytotoxic extracellularly, but once incorporated into cells, it can induce cell death rapidly (Chaudhary et al. 1990; Ogata et al. 1990; Song et al. 2005). CPPs can simply be identified using PSIF-mediated cytotoxicity as an index. In this study, we attempted to create novel CPPs, with greater transduction efficiency cell-penetrating mechanisms that differ from existing CPPs, using a random peptide phage library and a screening system with PSIF.

Table 1: Amino acid sequence of 9 clones selected from random 18 mer peptide library

Clone	Sequence
1	Y A Q Y K I T T A S P G D V K T S N
2	T Y A W Q Y C Q R T G R A L P N T K
3	R K H D A M D S T R R C W P H A P C
4	H N Q R H V K N W P D G F Q R N W S
5	K E Q K N P Q K Q F S S R G P A P N
6	Y P R Y K L Q D T V Q D R L R H R H
7	P K D A Q A S Y T P N N F N L S T T
8	M R Q P K P D T S N Y K D R V K S S
9	M F K G A F T Q Y H S T H E S T E N

2. Investigations, results and discussion

In a first step, a random 18mer peptide phage library was constructed in consideration of cell membrane thickness and the length of existing CPPs. We confirmed that the diversity of the library was 2.0×10^6 CFU, and 9 randomly selected clones consisted of different amino acids as shown by sequence analysis (Table 1). Cell panning was then performed using this library to select clones binding to A431 cells. We evaluated the efficacy of cell panning by calculating the ratio of input to output phage. With successive panning rounds, the ratio of output phage to input phage was increased by approximately 72-fold (Fig. 1). This data suggests that the number of peptide-displaying phages bound to A431 cells was increased. Phagemids of the phage clones selected by cell panning were collected, and the genes encoding peptides were recombined into the PSIF fusion peptide expression vector.

PSIF, which is non-toxic outside the cell, is highly cytotoxic: it inhibits protein synthesis even when only a few molecules are released into the cytosol. PSIF fusion peptides were produced in culture medium of *E. coli*, and applied to A431 cells. We examined the transduction efficacy of peptides into cytoplasm as an index of cytotoxicity of peptide-PSIF fusion protein (Fig. 2). The viability of cells treated with PSIF fusion peptide was calculated by setting

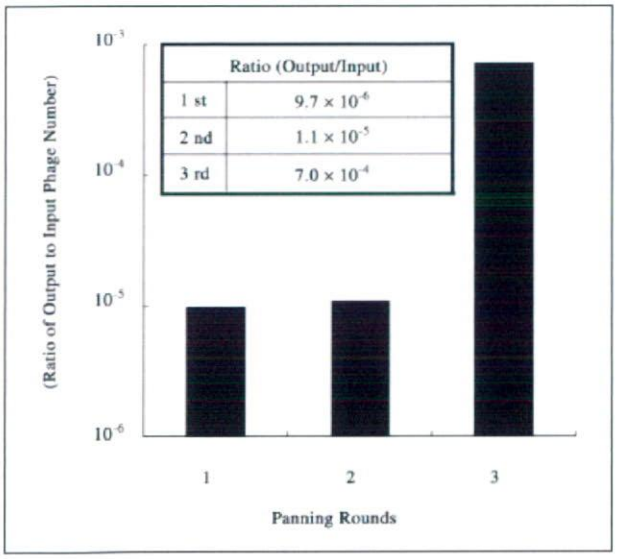

Fig. 1: Selection of binding and internalized phage clones by panning to A431. Phage clones binding to A431 cells with high affinity were collected. The ratio (output phage/input phage) in 3 rounds of panning was calculate. The number of phage clones binding to A431 cells increased with successive rounds of panning

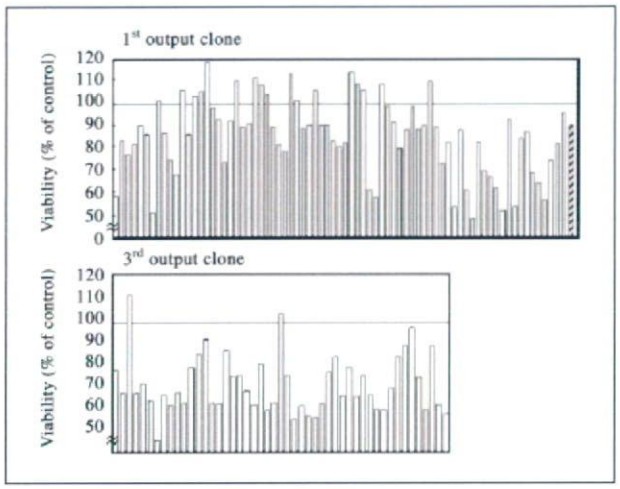

Fig. 2: Cytotoxic activity of randomly selected clones from a random 18mer peptide library. Phage clones were collected after 1 or 3 rounds of panning and genes encoding peptides were recombined with PSIF expression vector. Cytotoxicity mediated by PSIF fusion peptide from randomly selected clones was measured by MTT assay in A431 cells. The viability of A431 cells treated with PSIF fusion TAT peptide was 100%. Clones: (open bar), TAT13: (filled bar)

the viability treated with PSIF fusion TAT peptide at 100%. The rate of clones with viability less than 80% in the first panning output was 16 out of 75 clones (21.3%), and in the third panning it was 28 out of 49 clones (57.1%). We selected 8 clones that introduced PSIF most effectively into the cell, and assessed their cytotoxicity for reproducibility (Fig. 3). The cellular uptake of all PSIF fusion peptides was greater than that of TAT peptide, and their amino acid sequences were analyzed. We then analyzed the phagemid sequences and identified 7 peptides that consisted of different amino acids (Table 2). Existing CPPs consist mainly of basic amino acids and are positively-charged so that they interact with the negatively-charged surface of the cell membrane (Tyagi et al. 2001; Vives et al. 1997; Ziegler and Seelig 2004), and this interaction is important for translocation. Interestingly, 7 peptides were mainly composed of hydrophobic amino acids and contained very few basic amino acids such as lysine and arginine, and were not positively-charged. It has also been reported that cell surface binding of cationic TAT

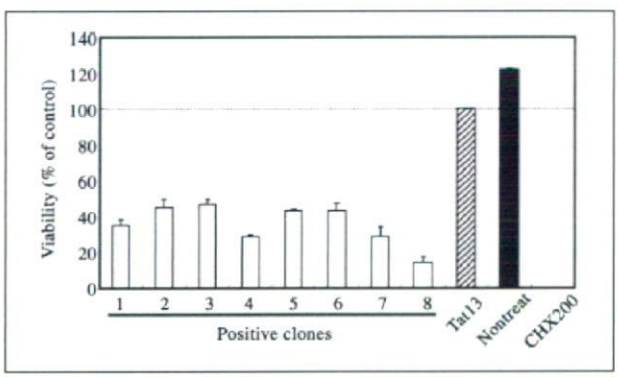

Fig. 3: Cytotoxic activity of positive clones. Positive clones were evaluated with TAT13-PSIF. Eight clones showing strong cytotoxic activity were identified and cytotoxic activity was measured by MTT assay. The viability of A431 cells treated with PSIF fusion TAT peptide was 100%, and the viability of cells treated with 200 mg/ml cycloheximide (CHX200) as a positive control was 0%. Clones: (open bar), TAT13: (hatched bar), Nontreat: (filled bar)

Table 2: Amino acid sequence of positive clones selected by screening with PSIF from random 18 mer peptide library

Clone	Sequence
1	S G E H T N G P S K T S V R W V W D
2	S M T T M E F G H S M I T P Y K I D
3	Q D G G T W H L V A Y C A K S H R Y
4	M S D P N M N P G T L G S S H I L W
5	S P G N Q S T G V I G T P S F S N H
6/7	S S G A N Y F F N A I Y D F L S N F
8	G T S R A N S Y D N L L S E T L T Q
Tat13	G R K K R R Q R R R P P Q
Antennapedia	R Q I K I W F Q N R R M K W K K
VP22	N A K T R R H E R R R K L A I E R

peptide is inhibited by pentosan polysulfate (Rusnati et al. 2001), or heparin (Rusnati et al. 1999). Thus, these peptides might be taken up by different pathways than existing CPPs.

Flow cytometric analysis was performed on the 7 FITC-labeled peptides to evaluate transduction efficacy. The penetration of clones 3 and 6/7 in A431 cells was more than 90% greater than that of FITC-labeled TAT peptide (Fig. 4a). In HeLa cells, clone 6/7 was taken up more effectively than TAT peptides (Fig. 4b). Flow cytometry showed that FITC-labeled clone3 was taken up most effectively in A431 and confocal laser scanning microscopy showed was translocated in A431 cells to the same degree as TAT peptide (Fig. 5). However, results from flow cytometric analysis using FITC-labeled peptides differed from those of the MTT assay using PSIF fusion peptides. With respect to TAT peptide, the 7 peptides fused with PSIF as a cargo molecule were introduced more effectively than peptides fused with low-molecular-weight compound like

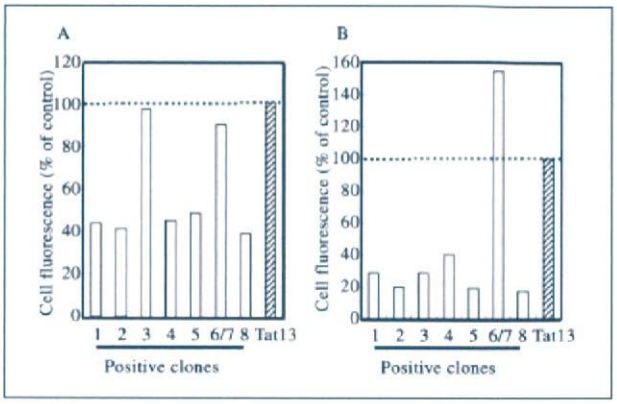

Fig. 4: Cellular uptake of positive clones in the cells. Positive clones were evaluated with FITC-labeled Tat13. A431 cells (A) or HeLa cells (B) were incubated with edium containing FITC-labeled peptide (1 mM) for 3 h. Intracellular translocated peptides were quantified with a a FACScan flow cytometer. Samples were treated with 0.25% trypsin before FACS analysis. The viability of A431 cells treated with PSIF fusion TAT peptide was 100%. Clones: (open bar), TAT13: (hatched bar)

FITC. These data suggest that the molecular weight of the cargo molecule has a considerable effect on the transduction efficiency of CPPs, depending on the characteristics and mechanism of penetration of the CPPs.

In this study, we used a random 18mer peptide library with a PSIF screening system to successfully create novel CPPs that efficiently introduced proteins into cells. We are now investigating the mechanism of penetration of these peptides in studies using inhibitors of cellular uptake pathways. We are also attempting to clarify the relationship between molecular weight of cargo molecules and transduction efficiency with several CPPs. Our data may contribute to the development of intracellular therapy with disease-related proteins.

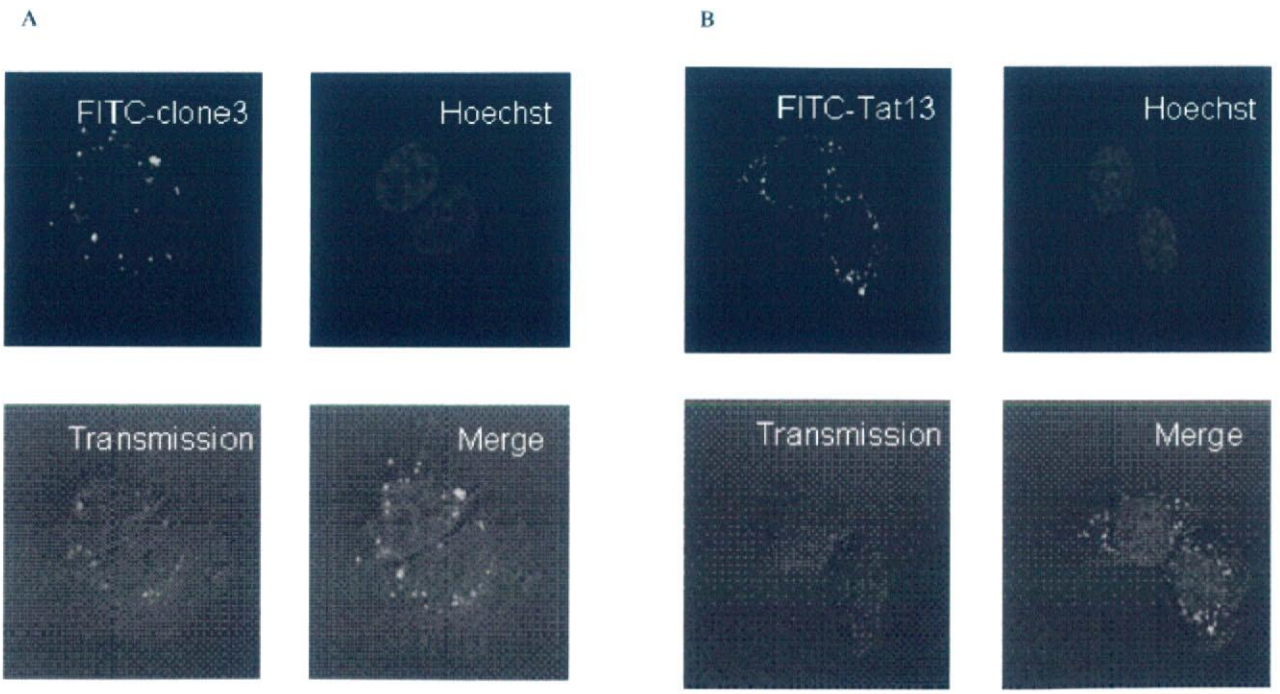

Fig. 5: Intracellular distribution of clone3 in living cells. A431 cells were cultured with FITC-labeled clone3 (A) or TAT peptide (B) for 3 h. Cells were washed and nuclei were stained with Hoechst 33342. Cells were examined by confocal laser microscopy

3. Experimental

3.1. Construction of gene fragment library coding random 18mer amino acids peptide

Gene fragments encoding random 18mer amino acid peptides were produced with Klenow fragment and the following primers: P-oligo1 (5′-GATTACGCCAAGCTTTGGAGCCTTTTTTTTGGAGATTTTCAACGTGAAAAAATTATTATTCGCAATTCCTTTAGTTGTTCCTTTCTATGCGGCCCAGCCGGCCATGGCC-3′), P-oligo4(5′-CGGCGCACCTGCGGCCGCSNNSNNSNNSNNSNNSNNSNNSNNSNNSNNSNNSNNSNNSNNSNNSNNGGCCATGGCCGGCTGGGCCGCATAGAA-3′).

To anneal the primers, 25 pmol each of P-oligo1 and P-oligo4 were mixed with 10 × Klenow buffer and incubated at 96 °C for 10 min, 70 °C for 5 min, and 16 °C for 10 min. Klenow fragment (TOYOBO) and 10 mM dNTP were then added to the reaction mixture and incubation was continued at 37 °C for 1 h. The purified sample was extracted from agarose gel using a QIAquick Gel Extraction Kit (QIAGEN). Gene fragments were then amplified by PCR. PCR reactions were cycled 35 times at 96 °C for 1 min, 65 °C for 1 min, 68 °C for 1 min, using pCANTAB HindIII (5′-GGAAACAGCTATGACCATGATTACGCCAAG-3′), and NotI extension (5′-GTAAATGAATTTTCTGTATGAGG-3′) as primers. The gene library and pCANTAB5E phagemid vector were digested with Hind III and Not I, and ligated with T4 ligase to display random 18mer amino acid peptides on the phage surface as fusion proteins with gene 3 protein. The phage library was prepared as previously described. Sequence analysis of randomly selected clones was performed.

3.2. Cell panning

A431 cells (epidermoid carcinoma, human) were maintained in Dulbecco's modified Eagle's medium supplemented with 10% fetal bovine serum (FBS) and 1% antibiotics. A431 cells (1.0×10^6 cells/2 ml/well) were seeded in 6-well plates and grown for 24 h. The wells were washed three times with PBS, and then incubated at 37 °C for 2 h with 2 ml/well Opti-MEM®I Reduced-Serum Medium (Invitrogen™ Life Techologies) containing 2% BSA. Medium was removed from each well, and the cells were incubated at 37 °C for 2 h with the purified phage library ready blocked with Opti-MEM containing 2% BSA. After washing the wells with PBS 20 times, the bound phages were eluted by incubating the wells with 100 mM HCl solution at 4 °C for 10 min. Eluted phages were immediately neutralized with 1 M Tris-HCl buffer pH 8.0 and were recovered as output phages. For the next panning, the eluted solution was added to log phase *E. coli* TG1 cells (Stratagene). The ratio of output phage to input phage was calculated to determine the effects of cell panning. Input phage and output phage were diluted in 2YT medium containing 50 μg/ml ampicillin and 2% glucose, and added to log phase *E. coli* TG1 cells. After incubation at 37 °C for 1 h, *E. coli* solution was seeded on LB (50 μg/ml ampicillin and 2% glucose) plates, and the number of colonies formed were counted.

3.3. Recombination to PSIF-expression vector

Protein synthesis inhibitory factor (PSIF, PE fragment) is an approximately 40kD fragment of the bacterial exotoxin (GenBank Accession No. K01397) derived from *Pseudomonas aeruginosa* (ATCC strain No. 29260). PSIF lacks its cell binding domain, and is the truncated form of *Pseudomonas aeruginosa* exotoxin, which is a non-toxic protein outside of the cell. One (Dr. Tsunoda) of us cloned the cDNA for PSIF from *Pseudomonas aeruginosa*, Migula by PCR using the primer set 5′-GAT GAT CGA TCg cgg ccg caG GTG CGC CGG TGC CGT ATC CGG ATC CGC TGG AAC CGC GTG CCG CAg act aca aag acg acg acg aca aaC CCG AGG GCG GCA GCC TGG CCG CGC TGA CC-3′ and 5′-GAT CGA TCG ATC act agt CTA cag ttc gtc ttt CTT CAG GTC CTC GCG CGG CGG TTT GCC GGG-3′. The fusion protein, denoted peptide-PSIF, consisted of peptide at the N-terminus and a PSIF at the C-terminus. First, the peptide gene containing phagemid vectors were recovered with QIAprep® Miniprep Kit (QIAGEN) and digested with HindIII and NotI. The peptide gene fragments encoding random 18mer amino acids were then subcloned into PSIF Expression Vector, which is modified from pCANTAB-5E.

3.4. Cytotoxicity assay by PSIF-fusion peptide

PSIF display phagemid was was transfected into TG1 cells, and individual TG1 clones were selected and grown at 37 °C in 96-well plates. Supernatants of TG1 cells were prepared for MTT assay. After seeding of A431 cells treated with 10 μg/ml cycloheximide at 2.0×10^4 cells/50 μl/well, 35 μL of Opti-MEM and 5 μl of supernatant were added to each well. After incubation at 37 °C for 24 h, 10 μL of 5 mg/ml MTT (3-(4,5-dimethylthiazol-2yl)-2,5-diphenyltetrazolium bromide) solution was added. MTT assays were carried out according to the manufacturer's protocol.

3.5. Flow cytometry

A431 and Hela cells (2.0×10^5 cells/well in 12-well plates) were grown for 24 h and incubated with each FITC-labeled clone peptide or TAT peptide at 37 °C for 3 h. The cells were washed twice with PBS and once with PBS/EDTA, and then treated with 0.25% trypsin for 10 min. The cells were collected, and fixed with PBS (500 μl/well) containing 1% PFA. The fluorescence intensities of the samples were measured with a FACS calibur (Becton Dickinson) detector.

3.6. Confocal laser scanning microscopy

Confocal laser scanning microscopy was performed using a Leica TCS SP2 (Leica). A431 cells were seeded at 2.25×10^4 cells/well in 4-well chamber slide glasses. After overnight incubation, cells were washed once with phenol red-free DMEM containing 10% FBC and 1% antibiotics. Each peptide (TAT peptide and clone3) and nuclear stain marker Hoechst33342 (molecular probes) were added at a concentration of 100 ng/ml in 500 μl of serum-free Opti-MEM), and then incubated at 37 °C for 3 h. The cells were subsequently washed three times and then analyzed.

Acknowledgements: This study was supported in part by Grants-in-Aid for Scientific Research (No. 17689008, 17016084, 17790135, 18015055, 18659047) from the Ministry of Education, Culture, Sports, Science and Technology of Japan, in part by Health and Labor Sciences Research Grant from the Ministry of Health, Labor and Welfare of Japan, in part by Health Sciences Research Grants for Research on Health Sciences focusing on Drug Innovation from the Japan Health Sciences Foundation, in part by Takeda Science Foundation, in part by Industrial Technology Research Grant Program (No. 03A47016a) from New Energy and Industrial Technology Development Organization (NEDO), and in part by JSPS Research Fellowships for Young Scientists (No. 08476, 08841, 09131) from the Japan Society for the Promotion of Science.

References

Astriab-Fisher A, Sergueev DS, Fisher M, Shaw BR, Juliano RL (2000) Antisense inhibition of P-glycoprotein expression using peptide-oligonucleotide conjugates. Biochem Pharmacol 60: 83–90.

Chaudhary VK, Jinno Y, FitzGerald D, Pastan I (1990) Pseudomonas exotoxin contains a specific sequence at the carboxyl terminus that is required for cytotoxicity. Proc Natl Acad Sci USA 87: 308–312.

Chung J, Park S, Kim D, Rhim J, Kim I, Choi I, Yi K, Ryu S, Suh P, Chung D, Bae Y, Shin Y (2002) Identification of antigenic peptide recognized by the anti-JL1 leukemia-specific monoclonal antibody from combinatorial peptide phage display libraries. J Cancer Res Clin Oncol 128: 641–649.

Connor CE, Norris JD, Broadwater G, Willson TM, Gottardis MM, Dewhirst MW, McDonnell DP (2001) Circumventing tamoxifen resistance in breast cancers using antiestrogens that induce unique conformational changes in the estrogen receptor. Cancer Res 61: 2917–2922.

Derossi D, Chassaing G, Prochiantz A (1998) Trojan peptides: the penetratin system for intracellular delivery. Trends Cell Biol 8: 84–87.

Elliott G, O'Hare P (1997) Intercellular trafficking and protein delivery by a herpesvirus structural protein. Cell 88: 223–233.

Frankel AD, Pabo CO (1988) Cellular uptake of the tat protein from human immunodeficiency virus. Cell 55: 1189–1193.

Green M, Loewenstein PM (1988) Autonomous functional domains of chemically synthesized human immunodeficiency virus tat trans-activator protein. Cell 55: 1179–1188.

Hou ST, Dove M, Anderson E, Zhang J, MacKenzie CR (2004) Identification of polypeptides with selective affinity to intact mouse cerebellar granule neurons from a random peptide-presenting phage library. J Neurosci Methods 138: 39–44.

Imai S, Mukai Y, Nagano K, Shibata H, Sugita T, Abe Y, Nomura T, Tsutsumi Y, Kamada H, Nakagawa S, Tsunoda S (2006) Quality enhancement of the non-immune phage scFv library to isolate effective antibodies. Biol Pharm Bull 29: 1325–1330.

Joliot A, Pernelle C, Deagostini-Bazin H, Prochiantz A (1991) Antennapedia homeobox peptide regulates neural morphogenesis. Proc Natl Acad Sci USA 88: 1864–1868.

Kuncl RW, Bilak MM, Bilak SR, Corse AM, Royal W, Becerra SP (2002) Pigment epithelium-derived factor is elevated in CSF of patients with amyotrophic lateral sclerosis. J Neurochem 81: 178–184.

Lambrechts D, Storkebaum E, Morimoto M, Del-Favero J, Desmet F, Marklund SL, Wyns S, Thijs V, Andersson J, van Marion I, Al-Chalabi A, Bornes S, Musson R, Hansen V, Beckman L, Adolfsson R, Pall HS, Prats H, Vermeire S, Rutgeerts P, Katayama S, Awata T, Leigh N, Lang-Lazdunski L, Dewerchin M, Shaw C, Moons L, Vlietinck R, Morrison KE, Robberecht W, Van Broeckhoven C, Collen D, Andersen PM, Carmeliet P (2003) VEGF is a modifier of amyotrophic lateral sclerosis in mice and humans and protects motoneurons against ischemic death. Nat Genet 34: 383–394.

Landon LA, Deutscher SL (2003) Combinatorial discovery of tumor targeting peptides using phage display. J Cell Biochem 90: 509–517.

Li Y, Rosal RV, Brandt-Rauf PW, Fine RL (2002) Correlation between hydrophobic properties and efficiency of carrier-mediated membrane transduction and apoptosis of a p53 C-terminal peptide. Biochem Biophys Res Commun 298: 439–449.

Mi Z, Lu X, Mai JC, Ng BG, Wang G, Lechman ER, Watkins SC, Rabinowich H, Robbins PD (2003) Identification of a synovial fibroblast-specific protein transduction domain for delivery of apoptotic agents to hyperplastic synovium. Mol Ther 8: 295–305.

Ogata M, Chaudhary VK, Pastan I, FitzGerald DJ (1990) Processing of Pseudomonas exotoxin by a cellular protease results in the generation of a 37,000-Da toxin fragment that is translocated to the cytosol. J Biol Chem 265: 20678–20685.

Okamoto T, Mukai Y, Yoshioka Y, Shibata H, Kawamura M, Yamamoto Y, Nakagawa S, Kamada H, Hayakawa T, Mayumi T, Tsutsumi Y (2004) Optimal construction of non-immune scFv phage display libraries from mouse bone marrow and spleen established to select specific scFvs efficiently binding to antigen. Biochem Biophys Res Commun 323: 583–591.

Rusnati M, Tulipano G, Spillmann D, Tanghetti E, Oreste P, Zoppetti G, Giacca M, Presta M (1999) Multiple interactions of HIV-I Tat protein with size-defined heparin oligosaccharides. J Biol Chem 274: 28198–28205.

Rusnati M, Urbinati C, Caputo A, Possati L, Lortat-Jacob H, Giacca M, Ribatti D, Presta M (2001) Pentosan polysulfate as an inhibitor of extracellular HIV-1 Tat. J Biol Chem 276: 22420–22425.

Scott JK, Smith GP (1990) Searching for peptide ligands with an epitope library. Science 249: 386–390.

Song S, Xue J, Fan K, Kou G, Zhou Q, Wang H, Guo Y (2005) Preparation and characterization of fusion protein truncated Pseudomonas Exotoxin A (PE38KDEL) in Escherichia coli. Protein Expr Purif 44: 52–57.

St Croix B, Rago C, Velculescu V, Traverso G, Romans KE, Montgomery E, Lal A, Riggins GJ, Lengauer C, Vogelstein B, Kinzler KW (2000) Genes expressed in human tumor endothelium. Science 289: 1197–1202.

Tyagi M, Rusnati M, Presta M, Giacca M (2001) Internalization of HIV-1 tat requires cell surface heparan sulfate proteoglycans. J Biol Chem 276: 3254–3261.

Vives E, Brodin P, Lebleu B (1997) A truncated HIV-1 Tat protein basic domain rapidly translocates through the plasma membrane and accumulates in the cell nucleus. J Biol Chem 272: 16010–16017.

Wadia JS, Dowdy SF (2002) Protein transduction technology. Curr Opin Biotechnol 13: 52–56.

Ziegler A, Seelig J (2004) Interaction of the protein transduction domain of HIV-1 TAT with heparan sulfate: binding mechanism and thermodynamic parameters. Biophys J 86: 254–263.

Available online at www.sciencedirect.com
ScienceDirect
Biochemical and Biophysical Research Communications 363 (2007) 1027–1032
BBRC
www.elsevier.com/locate/ybbrc

Improved cytosolic translocation and tumor-killing activity of Tat-shepherdin conjugates mediated by co-treatment with Tat-fused endosome-disruptive HA2 peptide

Toshiki Sugita [a,b], Tomoaki Yoshikawa [a], Yohei Mukai [a,b], Natsue Yamanada [a,b], Sunao Imai [a,b], Kazuya Nagano [a,b], Yasunobu Yoshida [a,c], Hiroko Shibata [a], Yasuo Yoshioka [a,d], Shinsaku Nakagawa [b], Haruhiko Kamada [a,d], Shin-ichi Tsunoda [a,d,*], Yasuo Tsutsumi [a,c,d]

[a] *Laboratory of Pharmaceutical Proteomics, National Institute of Biomedical Innovation, 7-6-8 Saito-Asagi, Ibaraki, Osaka 567-0085, Japan*
[b] *Department of Biotechnology and Therapeutics, Graduate School of Pharmaceutical Sciences, Osaka University, 1-6 Yamadaoka, Suita, Osaka 565-0871, Japan*
[c] *Department of Biomedical Innovation, Graduate School of Pharmaceutical Sciences, Osaka University, 1-6 Yamadaoka, Suita, Osaka 565-0871, Japan*
[d] *The Center for Advanced Medical Engineering and Informatics, Osaka University, 1-6 Yamadaoka, Suita, Osaka 565-0871, Japan*

Received 6 September 2007
Available online 29 September 2007

Abstract

Tat peptides are useful carriers for delivering biologic molecules into the cell for both functional analysis of intracellular disease-related proteins and treatment of refractory diseases. Most internalized Tat-fused cargos (Tat-cargos) are trapped within the endosome, however, which limits the biologic function of the cargo. In this study, we demonstrated that Tat-fused HA2 peptide ($HA2^{Tat}$), an endosome disrupted peptide, enhanced the endosome-escape efficiency of Tat-cargos. In cells treated with a mixture of fluorescein isothiocyanate-labeled Tat and $HA2^{Tat}$, widespread fluorescence was observed throughout the cytosol. In addition, this $HA2^{Tat}$-mediated cytosolic delivery technique led to enhanced cytotoxicity of Tat-fused anti-cancer peptides, specifically shepherdin. Thus, we improved the function of the delivered molecules by co-treating with $HA2^{Tat}$ and propose that this is a useful method for the delivery of therapeutic macromolecules into the cytosol.

Keywords: Tat; HA2; Protein transduction domain; PTD; Shepherdin; Peptidomimetic antagonist; Peptide blocker

Progress in genomics and proteomics research has led to an increased need for functional annotation of proteomes to allow for the rational choice of particular therapeutic targets from a growing set of candidates. At the same time, the emergence of the interactome of intracellular proteins, such as signal transduction- and protein transport-related proteins, will continue to generate tremendous candidate interactions whose functions need to be clarified and validated in relation with disease [1]. Although small interference RNA- or antisense oligonucleotide-mediated gene knockdown technology are invaluable as primary tools for validation analysis [2,3], these techniques are not always useful for true functional proteomics, because they are not suitable for analysis of post-transcriptional modification, such as phosphorylation, transport to organelles, and protein degradation, and the findings do not always correlate with transcript levels. Therefore, alternative technologies are needed to clarify the function of intracellular candidates, not at the transcript level but at the protein level. Progress in this field will lead to the development of various therapeutic agents.

* Corresponding author. Address: Laboratory of Pharmaceutical Proteomics, National Institute of Biomedical Innovation, 7-6-8 Saito-Asagi, Ibaraki, Osaka 567-0085, Japan. Fax: +81 72 641 9817.
E-mail address: tsunoda@nibio.go.jp (S. Tsunoda).

0006-291X/$ - see front matter © 2007 Elsevier Inc. All rights reserved.
doi:10.1016/j.bbrc.2007.09.077

Specific inhibition of protein–protein interactions by peptide-blockers, i.e., protein fragments, is a powerful methodology for investigating target validation at the protein level [4–6]. Furthermore, these peptide-blockers possess the potential to be used directly as therapeutic agents. Because many validation targets exist in the cell, it is important that peptide-blockers be delivered directly into cells. There are several recent reports of potent delivery vehicles, known as protein transduction domains (PTD), that can deliver bulky molecular cargos, such as peptides, proteins, oligonucleotides, and nano-particles, into a wide variety of cell types [7–9]. The best-known example of a PTD is the 11 amino acid sequence (Tat; YGRKKRRQRRR) derived from the human immunodeficiency virus type 1 (HIV-1)-Tat protein, and Tat-mediated delivery of peptide-blockers is thought to be useful for evaluating intracellular candidate proteins and developing peptide-based novel therapeutic drugs [10,11]. Recent studies suggested that Tat-fused cargo import is mediated by endocytotic pathways, such as lipid raft-dependent macropinocytosis [12,13]. After internalization via the macropinocytotic pathway, cargos are carried to macropinosomes. For molecules delivered by Tat to function in the cell as both validation probes and therapeutic drugs, they must reach the cytosol. Therefore, macropinosomal escape techniques are needed for the Tat-mediated intracellular delivery of peptide-blockers.

In this context, in the present study we investigated whether the effect of co-treatment with Tat-fused endosome-disruptive peptide ($HA2^{Tat}$) and Tat-fused anti-cancer peptide-blocker shepherdin ($shepherdin^{Tat}$) induced delivery into the cytosol of tumor cells and enhanced the anti-cancer effect of shepherdin. Although cancer cell treatment with shepherdin peptides, which interfere with the binding between heat shock protein 90 (Hsp90) and survivin, promote the degradation of survivin and increase the sensitivity to apoptosis [14], it is still possible that most of the treated peptides are entrapped in the macropinosomes, thereby limiting the function of shepherdin. With this in mind, we aimed to enhance the cytosolic delivery of peptide-blockers using the N-terminal 20 amino acid peptide of the influenza virus hemagglutinin protein (HA2). HA2 is well-characterized as a pH-sensitive membrane-disruptive peptide that destabilizes lipid membranes at low pH [15,16], and a recent study showed that Tat-fused with HA2 ($HA2^{Tat}$) markedly enhances the disruption of macropinosomes [12]. Therefore, we hypothesized that co-treatment with $HA2^{Tat}$ and Tat-fused peptide-blocker $shepherdin^{Tat}$ will be a promising approach for validating intracellular targets from proteomics analysis as well as the development of effective peptide-based anti-cancer drugs. Here, we evaluated the utility of this strategy using shepherdin peptides.

Materials and methods

Cell lines. HeLa cells, human cervical carcinoma cells, and A549 cells, human lung non-small-cell carcinoma cells, were obtained from the American Type Culture Collection (Manassas, VA). HeLa cells were cultured in α-minimal essential medium (MEMα; Wako Pure Chemical, Osaka, Japan) medium supplemented with 10% fetal bovine serum (FBS) and antibiotics. A549 cells were maintained in Dulbecco's modified Eagle's medium (Wako Pure Chemical) supplemented with 10% FBS, 1% L-glutamine, and antibiotics. These cells were cultured at 37 °C, 5% CO_2.

Synthetic peptides. All peptides used in the present study were purchased from GL Biochem Ltd. (Hiroshima, Japan) and their purities of 90% or more were confirmed by HPLC analysis and mass spectroscopy. The sequences of these peptides were YGRKKRRQRRRK-FITC for Tat-fused fluorescein isothiocyanate ($FITC^{Tat}$), GLFEAIEGFIENGWEG MIDGWYGYGRKKRRQRRR for HA2-fused Tat ($HA2^{Tat}$), KHSSG CAFL for shepherdin, and KHSSGCAFLYGRKKRRQRRR for shepherdin-fused Tat ($shepherdin^{Tat}$). The Tat sequence is underlined.

Intracellular localization analysis. HeLa cells were cultured on chamber coverglass (Nunc International, Naperville, IL) at 3.0×10^4 cells/well in MEMα supplemented with 10% FBS and incubated for 24 h at 37 °C. Peptide internalization was performed as follows. HeLa cells were co-treated with $FITC^{Tat}$ (10 μM) with or without $HA2^{Tat}$ (2 μM) in Opti-MEM I (Invitrogen, CA) containing 100 ng/ml Hoechst 33342 (Invitrogen). After incubation at 37 °C for 6 h, the medium was replaced with fresh medium and the fluorescence was observed by confocal laser scanning microscopy (Leica Microsystems GmbH, Germany) without cell fixation.

Cytotoxicity assay. HeLa or A549 cells were seeded on 96-well tissue culture plates (Nunc) at 1.0×10^4 cells/well. After incubation for 24 h at 37 °C, the cells were co-treated with various concentrations of shepherdin or $shepherdin^{Tat}$ in the presence or absence of 2 μM (for HeLa cells) or 5 μM (for A549 cells) $HA2^{Tat}$. After 6 h incubation, cell viability was measured using a WST-8 assay kit (Nacalai Tesque, Kyoto, Japan) according to the manufacturer's instructions.

Flow cytometry analysis. HeLa or A549 cells were seeded on 24-well tissue culture plates (Nunc) at 1.0×10^5 cells/well for 24 h at 37 °C. The cells were co-treated with 10 μM $FITC^{Tat}$ in the presence of 2 μM (for HeLa cells) or 5 μM (for A549 cells) $HA2^{Tat}$ diluted in Opti-MEM I for 6 h. Cells were washed three times with 1 mM EDTA in PBS and treated with 0.25% trypsin to remove the $FITC^{Tat}$ adsorbed on the cell surface and to harvest the cells. Fluorescence was analyzed on a FACSCalibur flow cytometer, and data were analyzed using CellQuest software (Becton–Dickinson, San Jose, CA).

Results and discussion

We first analyzed the subcellular localization of $FITC^{Tat}$ by confocal laser scanning microscopy (Fig. 1). In HeLa cells treated with $FITC^{Tat}$ alone, only punctuate fluorescence was observed intracellularly. We previously confirmed that Tat peptides co-localized in live cells to vesicles with FM4-64, which is a general endosome marker (data not shown). Together, this result and the previous observation indicate that Tat-cargo enters the cell by endocytosis, but most of it is entrapped within the endosomal vesicles. As these results demonstrated that Tat-cargo accumulated in the endosomal vesicles, which severely limited its function, a method that enhances the escape of the Tat-cargo from the endosomes into the cytosol is indispensable for the cargo to exert its function.

Recently, a method for the intracellular delivery of Tat-fused biologically active protein using membrane-disruptive HA2 was studied by several researchers. Wadia et al. reported that $HA2^{Tat}$ markedly enhanced the recombination activity of Tat-fused Cre protein [12]. Additionally, Michiue et al. succeeded in enhancing both nuclear transportation and transcription activity of PTD-fused p53,

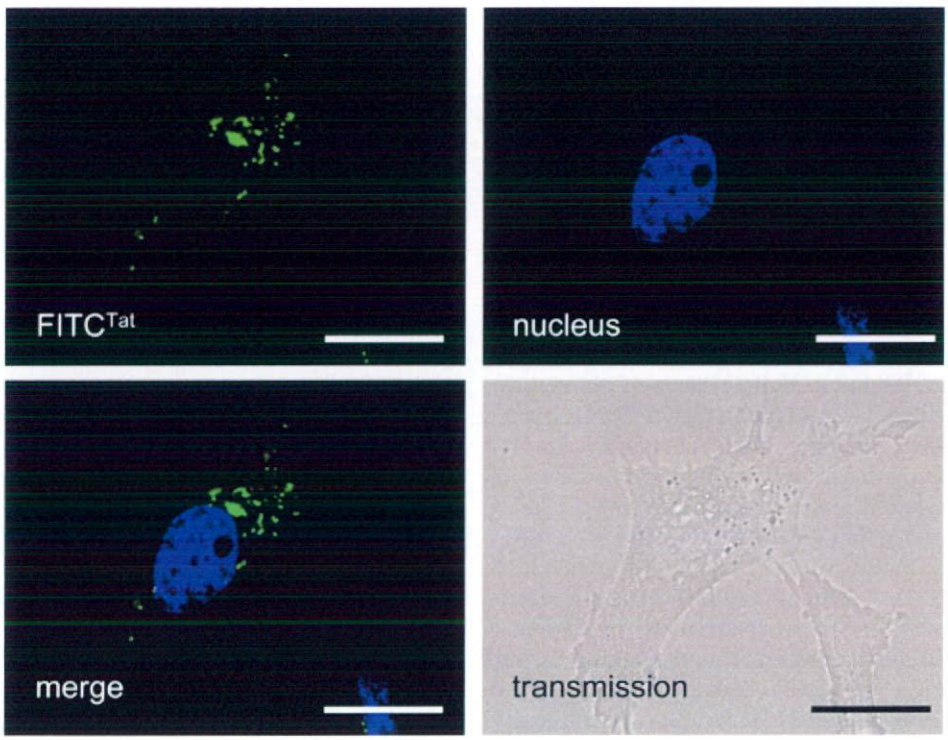

Fig. 1. Intracellular distributions of FITC^{Tat}. HeLa cells were treated with 10 μM FITC^{Tat} alone, and cultured for 6 h. Fluorescence images were acquired by confocal laser scanning microscopy and the signals were digitally merged. The nucleus was counterstained with Hoechst 33342 (blue). Scale bars in each microphotograph indicate 20 μm.

which was directly linked with HA2 [17]. To the best of our knowledge, however, there has been no direct demonstration that HA2 enhances the escape of Tat-cargo from endosomal vesicles. To investigate whether co-treatment with HA2^{Tat} effectively induces the cytosolic translocation of Tat-cargo, HeLa cells were co-treated with HA2^{Tat} and FITC^{Tat} and subcellular localization of FITC^{Tat} was analyzed by confocal laser scanning microscopy (Fig. 2A). The majority of FITC^{Tat} was entrapped in endosomes (Fig. 1). In contrast, co-treatment of HeLa cells with FITC^{Tat} and HA2^{Tat} resulted in dispersed distribution of fluorescence, indicating cytosolic translocation of the Tat-cargo due to disruption of the endosomal vesicles (Fig. 2A). In addition, co-treatment with HA2^{Tat} did not affect the transduction efficiency of FITC^{Tat}, compared with cells treated with FITC^{Tat} alone (Fig. 2B). Thus, we demonstrated that HA2^{Tat} enhances the endosome-escape of Tat-cargos without influencing internalization efficiency.

The model peptide-blocker; survivin-derived shepherdin was developed from a peptidomimetic antagonist of the complex between Hsp90 and survivin [14]. Because knock-down of survivin mRNA induces tumor cell death, survivin is suggested to have a crucial role in tumor development [18,19]. A critical point for the survivin function in tumor cells is its association with Hsp90, which is required to preserve survivin stability [20]. Although transduction of PTD-fused shepherdin (shepherdin^{PTD}) into cancer cells could induce tumor cell death, a high concentration of shepherdin^{PTD} is needed for the induction of growth inhibition in various cancer cells [14]. Therefore, here we used the shepherdin peptide as a model peptide-blocker to investigate the utility of HA2^{Tat}-mediated cytosolic delivery.

The effects of co-treatment with HA2^{Tat} and increasing concentrations of shepherdin^{Tat} on cell viability were investigated using HeLa and A549 cells, which highly express survivin protein [21]. Cells treated with shepherdin alone or co-treated with shepherdin and HA2^{Tat} grew vigorously (Fig. 3). Shepherdin^{Tat} markedly inhibited growth in both HeLa and A549 cells. Co-treatment with HA2^{Tat} and shepherdin^{Tat}, in contrast, resulted in a greater dose-dependent growth inhibition effect than the cells treated with shepherdin^{Tat} alone. The IC_{50} value of co-treatment with HA2^{Tat} and shepherdin^{Tat} (HeLa; 15.61 μM and A549; 32.89 μM) was at least 3-times lower than that of shepherdin^{Tat} alone (HeLa; 48.98 μM and A549; >100 μM; Table 1). These observations indicated that HA2^{Tat} markedly enhanced the cytosolic release of the cargo and the shepherdin-mediated anti-tumor effect. In addition, lung-derived normal human microvascular blood vessel endothelial cells co-treated with HA2^{Tat} and shepherdin^{Tat} showed little growth inhibition (data not shown). Survivin is strongly expressed in embryonic and fetal organs and nearly every human tumor, but has not been reported in differentiated normal tissues [19,22]. Therefore, shepherdin could exert tumor-selective cytotoxic activity. On the other hand, the data presented in Fig. 3 show that HeLa cells are more sensitive to shepher-

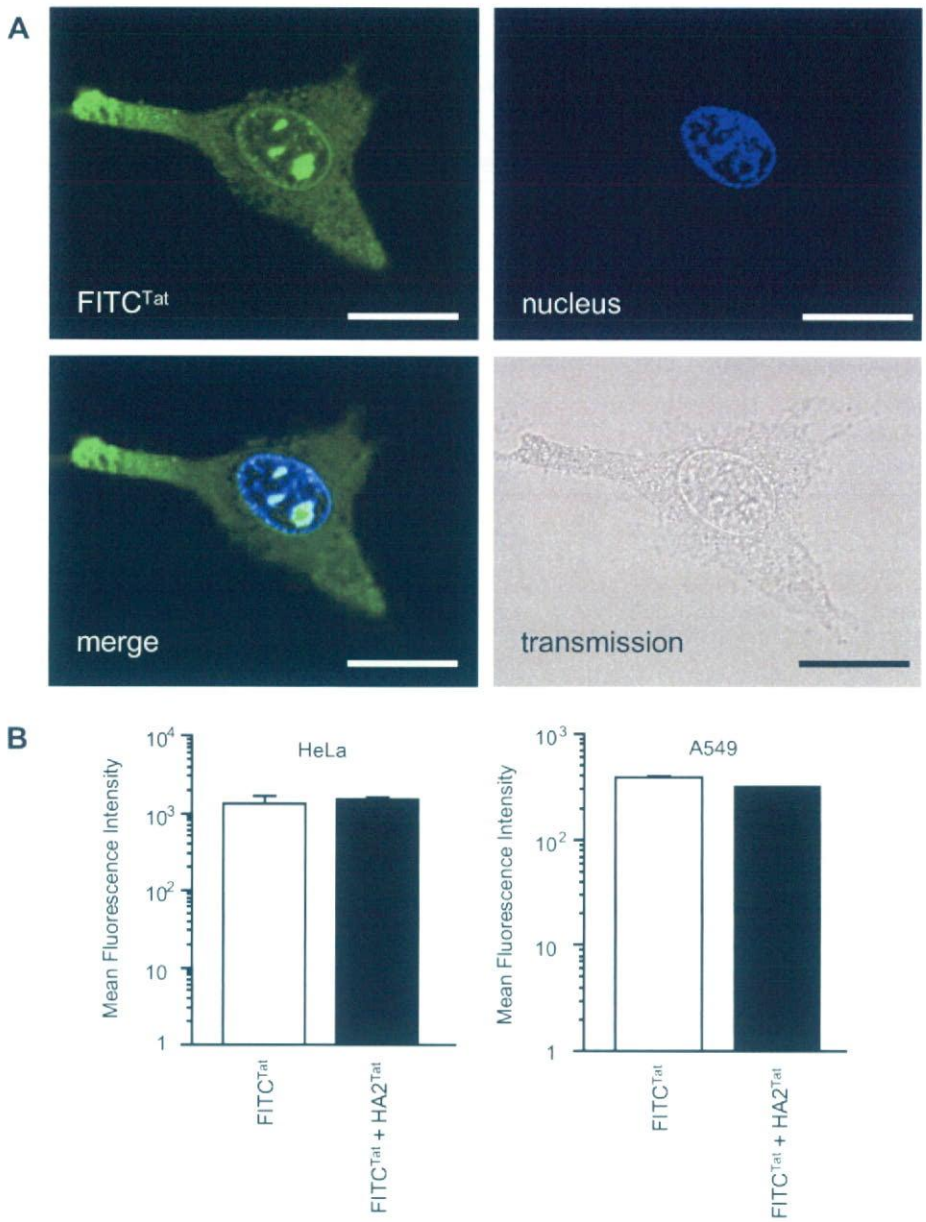

Fig. 2. $HA2^{Tat}$ enhances endosome escape efficiency without influencing the cellular uptake of $FITC^{Tat}$. (A) HeLa cells were treated with 10 μM $FITC^{Tat}$ in the presence of 2 μM $HA2^{Tat}$ for 6 h. The localization of $FITC^{Tat}$ was observed by confocal laser scanning microscopy. The nucleus was counterstained with Hoechst 33342 (blue). Scale bar = 20 μm. (B) HeLa or A549 cells were treated with 10 μM $FITC^{Tat}$ in the presence of 2 μM (for HeLa cells; A) or 5 μM (for A549 cells; B) $HA2^{Tat}$ for 6 h. After trypsin treatment to digest adsorbed-peptides on the cell surface, cells were harvested and analyzed by flow cytometry. Error bars indicate means ± SD of triplicate assays.

din^{Tat} compared with A549 cells. One possibility is the transduction efficiency of $shepherdin^{Tat}$ is different between HeLa and A549 cells. In fact, Fig. 2B shows that the mean fluorescence intensity of $FITC^{Tat}$-treated HeLa cells was relatively higher than that of A549 cells. Nevertheless, almost the same level of growth inhibition was observed in HeLa and A549 cells that were co-treated with $HA2^{Tat}$ and $shepherdin^{Tat}$. Therefore, this $HA2^{Tat}$-mediated cytosolic peptide delivery technique is very useful because it is not affected by cell type.

In the present study, we demonstrated that co-treatment with $HA2^{Tat}$ enhances cytosolic release of Tat-fused peptide-blockers and its biologic activity. Although this co-treatment method is highly useful for enhancing cytosolic peptide delivery, the efficiency of the Tat-mediated intracellular transduction was slightly affected by cell type. Thus, we are currently working to create versatile and highly transducible PTDs using our original PTD-rearrangement method with a phage-displayed random peptide library [23,24].

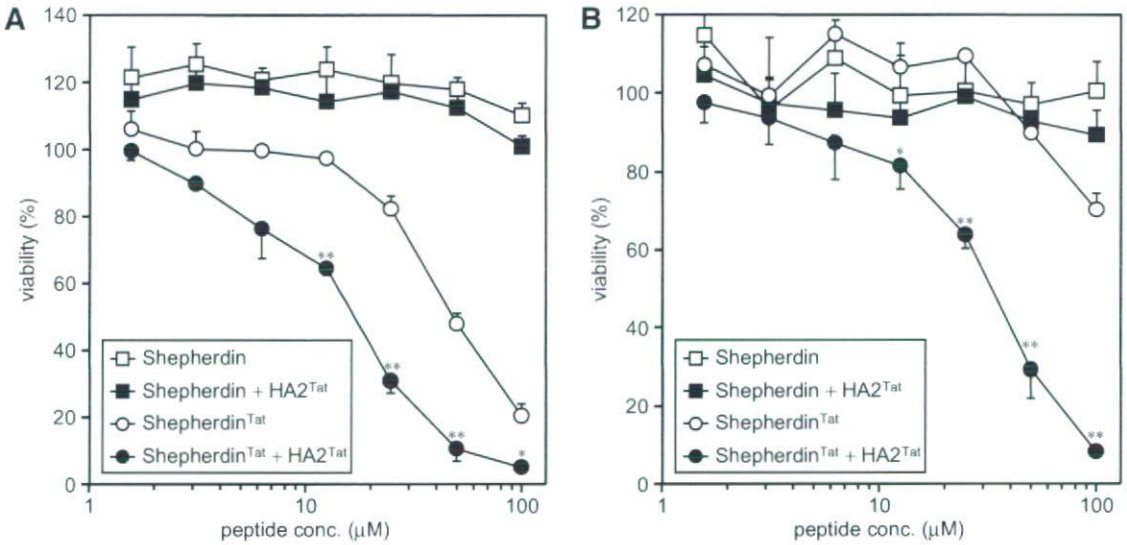

Fig. 3. $HA2^{Tat}$ enhances the cytotoxicity of shepherdin^{Tat}. The cells were treated with shepherdin or shepherdin^{Tat} in the presence of 2 μM (for HeLa cells; A) or 5 μM (for A549 cells; B) $HA2^{Tat}$. After 6 h, the cell viability was analyzed by WST-8 assay. Data are presented as means ± SD of triplicate assays. ** and *, $p < 0.001$ and <0.005, respectively (versus shepherdin^{Tat}).

Table 1
Cytotoxicity of shepherdin^{Tat} in HeLa and A549 Cells

Cell	Peptide	IC_{50} (μM)
HeLa	Shepherdin^{Tat}	48.98
	Shepherdin^{Tat} + $HA2^{Tat}$	15.61
A549	Shepherdin^{Tat}	>100
	Shepherdin^{Tat} + $HA2^{Tat}$	32.89

Acknowledgments

This study was supported in part by Grants-in-Aid for Scientific Research (17689008) from the Ministry of Education, Culture, Sports, Science and Technology of Japan; in part by Health and Labor Sciences Research Grant (from the Ministry of Health, Labor and Welfare of Japan, in part by Grant for Industrial Technology Research Program (03A47016a) from New Energy and Industrial Technology Development Organization (NEDO) of Japan; and in part by Japan Society for the Promotion of Science (JSPS) Research Fellowships for Young Scientists (No. 08841) from the JSPS.

References

[1] U. Stelzl, U. Worm, M. Lalowski, C. Haenig, F.H. Brembeck, H. Goehler, M. Stroedicke, M. Zenkner, A. Schoenherr, S. Koeppen, J. Timm, S. Mintzlaff, C. Abraham, N. Bock, S. Kietzmann, A. Goedde, E. Toksoz, A. Droege, S. Krobitsch, B. Korn, W. Birchmeier, H. Lehrach, E.E. Wanker, A human protein–protein interaction network: a resource for annotating the proteome, Cell 122 (2005) 957–968.

[2] L.M. Cullen, G.M. Arndt, Genome-wide screening for gene function using RNAi in mammalian cells, Immunol. Cell Biol. 83 (2005) 217–223.

[3] R. Kramer, D. Cohen, Functional genomics to new drug targets, Nat. Rev. Drug Discov. 3 (2004) 965–972.

[4] F.J. Mendoza, P.S. Espino, K.L. Cann, N. Bristow, K. McCrea, M. Los, Anti-tumor chemotherapy utilizing peptide-based approaches—apoptotic pathways, kinases, and proteasome as targets, Arch. Immunol. Ther. Exp. (Warsz) 53 (2005) 47–60.

[5] A.I. Archakov, V.M. Govorun, A.V. Dubanov, Y.D. Ivanov, A.V. Veselovsky, P. Lewi, P. Janssen, Protein–protein interactions as a target for drugs in proteomics, Proteomics 3 (2003) 380–391.

[6] A.V. Veselovsky, Y.D. Ivanov, A.S. Ivanov, A.I. Archakov, P. Lewi, P. Janssen, Protein–protein interactions: mechanisms and modification by drugs, J. Mol. Recognit. 15 (2002) 405–422.

[7] S.R. Schwarze, A. Ho, A. Vocero-Akbani, S.F. Dowdy, In vivo protein transduction: delivery of a biologically active protein into the mouse, Science 285 (1999) 1569–1572.

[8] G.P. Dietz, M. Bahr, Delivery of bioactive molecules into the cell: the Trojan horse approach, Mol. Cell Neurosci. 27 (2004) 85–131.

[9] A. Chauhan, A. Tikoo, A.K. Kapur, M. Singh, The taming of the cell penetrating domain of the HIV Tat: myths and realities, J. Control. Release 117 (2007) 148–162.

[10] T. Borsello, P.G. Clarke, L. Hirt, A. Vercelli, M. Repici, D.F. Schorderet, J. Bogousslavsky, C. Bonny, A peptide inhibitor of c-Jun N-terminal kinase protects against excitotoxicity and cerebral ischemia, Nat. Med. 9 (2003) 1180–1186.

[11] S.C. Pero, G.S. Shukla, M.M. Cookson, S. Flemer Jr., D.N. Krag, Combination treatment with Grb7 peptide and Doxorubicin or Trastuzumab (Herceptin) results in cooperative cell growth inhibition in breast cancer cells, Br. J. Cancer 96 (2007) 1520–1525.

[12] J.S. Wadia, R.V. Stan, S.F. Dowdy, Transducible TAT-HA fusogenic peptide enhances escape of TAT-fusion proteins after lipid raft macropinocytosis, Nat. Med. 10 (2004) 310–315.

[13] I.M. Kaplan, J.S. Wadia, S.F. Dowdy, Cationic TAT peptide transduction domain enters cells by macropinocytosis, J. Control. Release 102 (2005) 247–253.

[14] J. Plescia, W. Salz, F. Xia, M. Pennati, N. Zaffaroni, M.G. Daidone, M. Meli, T. Dohi, P. Fortugno, Y. Nefedova, D.I. Gabrilovich, G. Colombo, D.C. Altieri, Rational design of shepherdin, a novel anticancer agent, Cancer Cell 7 (2005) 457–468.

[15] X. Han, J.H. Bushweller, D.S. Cafiso, L.K. Tamm, Membrane structure and fusion-triggering conformational change of the fusion domain from influenza hemagglutinin, Nat. Struct. Biol. 8 (2001) 715–720.

[16] J.J. Skehel, K. Cross, D. Steinhauer, D.C. Wiley, Influenza fusion peptides, Biochem. Soc. Trans. 29 (2001) 623–626.
[17] H. Michiue, K. Tomizawa, F.Y. Wei, M. Matsushita, Y.F. Lu, T. Ichikawa, T. Tamiya, I. Date, H. Matsui, The NH2 terminus of influenza virus hemagglutinin-2 subunit peptides enhances the anti-tumor potency of polyarginine-mediated p53 protein transduction, J. Biol. Chem. 280 (2005) 8285–8289.
[18] H. Uchida, T. Tanaka, K. Sasaki, K. Kato, H. Dehari, Y. Ito, M. Kobune, M. Miyagishi, K. Taira, H. Tahara, H. Hamada, Adeno-virus-mediated transfer of siRNA against survivin induced apoptosis and attenuated tumor cell growth in vitro and in vivo, Mol. Ther. 10 (2004) 162–171.
[19] N. Zaffaroni, M. Pennati, M.G. Daidone, Survivin as a target for new anticancer interventions, J. Cell Mol. Med. 9 (2005) 360–372.
[20] P. Fortugno, E. Beltrami, J. Plescia, J. Fontana, D. Pradhan, P.C. Marchisio, W.C. Sessa, D.C. Altieri, Regulation of survivin function by Hsp90, Proc. Natl. Acad. Sci. USA 100 (2003) 13791–13796.
[21] P.C. Kuo, H.F. Liu, J.I. Chao, Survivin and p53 modulate quercetin-induced cell growth inhibition and apoptosis in human lung carcinoma cells, J. Biol. Chem. 279 (2004) 55875–55885.
[22] M.J. Duffy, N. O'Donovan, D.J. Brennan, W.M. Gallagher, B.M. Ryan, Survivin: a promising tumor biomarker, Cancer Lett. 249 (2007) 49–60.
[23] Y. Mukai, T. Sugita, T. Yamato, N. Yamanada, H. Shibata, S. Imai, Y. Abe, K. Nagano, T. Nomura, Y. Tsutsumi, H. Kamada, S. Nakagawa, S. Tsunoda, Creation of novel protein transduction domain (PTD) mutants by a phage display-based high-throughput screening system, Biol. Pharm. Bull. 29 (2006) 1570–1574.
[24] H. Kamada, T. Okamoto, M. Kawamura, H. Shibata, Y. Abe, A. Ohkawa, T. Nomura, M. Sato, Y. Mukai, T. Sugita, S. Imai, K. Nagano, Y. Tsutsumi, S. Nakagawa, T. Mayumi, S. Tsunoda, Creation of novel cell-penetrating peptides for intracellular drug delivery using systematic phage display technology originated from Tat transduction domain, Biol. Pharm. Bull. 30 (2007) 218–223.

THE JOURNAL OF BIOLOGICAL CHEMISTRY VOL. 283, NO. 2, pp. 998–1007, January 11, 2008

Creation and X-ray Structure Analysis of the Tumor Necrosis Factor Receptor-1-selective Mutant of a Tumor Necrosis Factor-α Antagonist*

Received for publication, September 21, 2007, and in revised form, November 2, 2007 Published, JBC Papers in Press, November 14, 2007, DOI 10.1074/jbc.M707933200

Hiroko Shibata,[a,b] Yasuo Yoshioka,[a,c] Akiko Ohkawa,[a] Kyoko Minowa,[a,d] Yohei Mukai,[a,e] Yasuhiro Abe,[a,e] Madoka Taniai,[f] Tetsuya Nomura,[a,e] Hiroyuki Kayamuro,[a,e] Hiromi Nabeshi,[a,e] Toshiki Sugita,[a,e] Sunao Imai,[a,e] Kazuya Nagano,[a,e] Tomoaki Yoshikawa,[a] Takuya Fujita,[d] Shinsaku Nakagawa,[c,e] Akira Yamamoto,[d] Tsunetaka Ohta,[f] Takao Hayakawa,[b] Tadanori Mayumi,[g] Peter Vandenabeele,[h] Bharat B. Aggarwal,[i] Teruya Nakamura,[j] Yuriko Yamagata,[j] Shin-ichi Tsunoda,[a,c] Haruhiko Kamada,[a,c1] and Yasuo Tsutsumi[a,c,e]

From the [a]National Institute of Biomedical Innovation, 7-6-8 Saito-Asagi, Ibaraki, Osaka 567-0085, Japan, [b]National Institute of Health Science, 1-18-1 Kamiyoga, Setagaya-ku, Tokyo 158-8501, Japan, [c]Center for Advanced Medical Engineering and Informatics, Osaka University, 1-6 Yamadaoka, Suita, Osaka 565-0871, Japan, [d]Kyoto Pharmaceutical University, Misasagi-Nakauchicho 5, Yamashina-ku, Kyoto 607-8414, Japan, [e]Graduate School of Pharmaceutical Sciences, Osaka University, 1-6 Yamadaoka, Suita, Osaka 565-0871, Japan, [f]Hayashibara Biochemical Laboratories, Inc., 1-2-3 Shimoishii, Okayama 702-8006, Japan, [g]Graduate School of Pharmaceutical Sciences, Kobe Gakuin University, 518 Arise, Igawadani, Nishi-ku, Kobe 651-2180, Japan, the [h]Department of Molecular Biomedical Research, Flanders Institute for Biotechnology and the Department of Molecular Biology, Ghent University, B-9052 Ghent, Belgium, the [i]Department of Experimental Therapeutics, University of Texas M. D. Anderson Cancer Center, Houston, Texas 77030, and [j]Faculty of Medical and Pharmaceutical Sciences, Kumamoto University, 5-1 Ooehonmachi, Kumamoto 862-0973, Japan

Tumor necrosis factor-α (TNF) induces inflammatory response predominantly through the TNF receptor-1 (TNFR1). Thus, blocking the binding of TNF to TNFR1 is an important strategy for the treatment of many inflammatory diseases, such as hepatitis and rheumatoid arthritis. In this study, we identified a TNFR1-selective antagonistic mutant TNF from a phage library displaying structural human TNF variants in which each one of the six amino acid residues at the receptor-binding site (amino acids at positions 84–89) was replaced with other amino acids. Consequently, a TNFR1-selective antagonistic mutant TNF (R1antTNF), containing mutations A84S, V85T, S86T, Y87H, Q88N, and T89Q, was isolated from the library. The R1antTNF did not activate TNFR1-mediated responses, although its affinity for the TNFR1 was almost similar to that of the human wild-type TNF (wtTNF). Additionally, the R1antTNF neutralized the TNFR1-mediated bioactivity of wtTNF without influencing its TNFR2-mediated bioactivity and inhibited hepatic injury in an experimental hepatitis model. To understand the mechanism underlying the antagonistic activity of R1antTNF, we analyzed this mutant using the surface plasmon resonance spectroscopy and x-ray crystallography. Kinetic association/dissociation parameters of the R1antTNF were higher than those of the wtTNF, indicating very fast bond dissociation. Furthermore, x-ray crystallographic analysis of R1antTNF suggested that the mutation Y87H changed the binding mode from the hydrophobic to the electrostatic interaction, which may be one of the reasons why R1antTNF behaved as an antagonist. Our studies demonstrate the feasibility of generating TNF receptor subtype-specific antagonist by extensive substitution of amino acids of the wild-type ligand protein.

Tumor necrosis factor (TNF)[2] is a major inflammatory cytokine that, like the other members of the TNF superfamily of ligands, plays a central role in host defense and inflammation (1). Elevated serum levels of TNF correlate with the severity and progression of the inflammatory diseases such as rheumatoid arthritis, inflammatory bowel disease, septic shock, multiple sclerosis, and hepatitis (2–4). So far, anti-TNF antibodies and soluble TNFRs, which interfere with the activity of TNF, have been used to treat various inflammatory diseases (5, 6). However, these therapies can cause serious side effects, such as bacterial and virus infection, lymphoma development, and lupus inflammatory disease (7–10), because they also inhibit the TNF-

* This work was supported in part by Grants-in-aid for Scientific Research 18015055, 18659047, and 7689008 from the Ministry of Education, Culture, Sports, Science and Technology of Japan and Japan Society for the Promotion of Science, by a Health Labor Sciences research grant from the Ministry of Health, Labor and Welfare of Japan, by Health Sciences research grants for research on health sciences focusing on drug innovation from the Japan Health Sciences Foundation, and in part by Japan Society for the Promotion of Science Research Fellowships for Young Scientists 02872, 08841, 09131. The costs of publication of this article were defrayed in part by the payment of page charges. This article must therefore be hereby marked "*advertisement*" in accordance with 18 U.S.C. Section 1734 solely to indicate this fact.

The atomic coordinates and structure factors (code 2E7A) have been deposited in the Protein Data Bank, Research Collaboratory for Structural Bioinformatics, Rutgers University, New Brunswick, NJ (http://www.rcsb.org/).

[1] To whom correspondence should be addressed: Laboratory of Pharmaceutical Proteomics, National Institute of Biomedical Innovation, 7-6-8 Saito-Asagi, Ibaraki, Osaka 567-0085, Japan. Fax: 81-72-641-9817; E-mail: kamada@nibio.go.jp.

[2] The abbreviations used are: TNF, tumor necrosis factor α; TNFR, TNF receptor; PDB, Protein Data Bank; PBS, phosphate-buffered saline; RT, reverse transcription; HUVEC, human umbilical vein endothelial cells; ELISA, enzyme-linked immunosorbent assay; GM-CSF, granulocyte-macrophage colony-stimulating factor; TES, 2-{[2-hydroxy-1,1-bis(hydroxymethyl)ethyl]amino}ethanesulfonic acid; EAE, experimental autoimmune encephalomyelitis; ALT, alanine aminotransferase; h, human; m, mouse; mut, mutant.

dependent host defense function of the patients. TNF blockade by administering these agents into patients with multiple sclerosis was also shown to aggravate their symptoms (11). Therefore, to overcome these problems, development of a new therapeutic strategy is highly desirable.

TNF binds to two receptor subtypes, p55 TNF receptor (TNFR1) and p75 TNF receptor (TNFR2), to exert its biological functions (12). Thus, functional analyses of the TNF receptors were carried out to explore a new therapeutic strategy. Previous studies using animal models of diseases such as arthritis and hepatitis demonstrated the predominant role of TNFR1 in the pathogenesis and exacerbation of inflammation (13, 14). In the experimental autoimmune encephalomyelitis model (EAE), which is widely used as an animal model of multiple sclerosis, the symptoms exacerbated significantly in the TNF knock-out mice compared with that in the wild-type mice (15). Another study indicates that the TNF has a dual role on the EAE model, an inflammatory and immunosuppressive effect, and although the immunosuppressive effect does not require the TNFR1, it is essential for the acute phase inflammation of EAE (16). On the other hand, although the TNFR1 is believed to be important for the defense mechanism against mycobacterium, the membrane-bound TNF, the prime activating ligand of TNFR2, was reported to be sufficient to control the mycobacterial infection (17, 18). Moreover, TNFR2 was shown to be crucial for the proliferation, activation, and antigen presentation of the T-cells, which are essential in the cell-mediated immune response against bacteria and virus (19–21). Therefore, blocking the TNFR1-mediated signal transduction emerged as a potential therapeutic strategy with low side effects for the inflammatory diseases.

From these perspectives, attempts were made to develop drugs targeted to TNFR1. Along with the progress of antibody engineering, attempts were made to develop an anti-TNFR1 antibody with antagonistic activity. But the desired antibody could not be created, because the anti-TNFR1 antibodies recognizing the TNF-binding site on TNFR1 acted like a TNFR1 agonist and not an antagonist (22). Attempts to design a low molecular weight TNFR1 antagonist based on the three-dimensional structural information of the TNFR1 was also not successful in identifying an antagonist that would selectively inhibit the TNF/TNFR1 interaction and would have sufficient therapeutic effect (23, 24). In this respect, we previously 1) constructed two phage libraries displaying the structural TNF variants in which six amino acid residues (amino acids 29, 31, 32, 145–147, library I; amino acids 84–89, library II) in the predicted receptor binding sites were replaced with other amino acid, 2) and we successfully identified the TNFR1-selective mutant with great biological activity from the library I.[3] In the screening process, mutants with high affinity for the TNFR1 and great TNFR1 selectivity were found from library II, although their biological activities were very weak.[3] The strategy described here could comprehensively assess the affinities and bioactivities of TNF variants, thus enabling the high-throughput screening of TNFR1-selective antagonists, which have no biological activity but high TNFR1 affinity. In this study, we analyzed the biological activity and TNFR1 affinity of 500 TNF variants, which were concentrated by panning against the TNFR1, and we subsequently isolated a novel TNFR1-selective antagonistic mutant TNF (R1antTNF). R1antTNF showed exclusive TNFR1 selectivity, and it efficiently inhibited wide varieties of TNFR1-mediated effects of the wild-type TNF *in vitro* and *in vivo*. Additionally, we used surface plasmon resonance and x-ray structural analyses to elucidate the underlying cause for the antagonist activity of R1antTNF.

EXPERIMENTAL PROCEDURES

Cell Culture—L-M cells (a mouse fibroblast cell line) were provided by Mochida Pharmaceutical Co. Ltd. (Tokyo, Japan) and were maintained in minimum Eagle's medium (Sigma) supplemented with 1% fetal bovine serum and 1% antibiotic mixture (penicillin 10,000 units/ml, streptomycin 10 mg/ml, and amphotericin B 25 μg/ml) (Nacalai Tesque, Kyoto, Japan). HEp-2 cells (a human fibroblast cell line) were provided by Cell Resource Center for Biomedical Research (Tohoku University, Sendai, Japan) and were maintained in RPMI 1640 medium (Sigma) supplemented with 10% fetal bovine serum and 1% antibiotic mixture (Nacalai Tesque). PC60-R1 and PC60-R2 cells (a mouse-rat fusion hybridoma consisting of human TNFR1- or TNFR2-transfected PC60 cells) were established as described previously (25) and maintained in RPMI 1640 medium supplemented with 10% fetal bovine serum, 1 mM sodium pyruvate, 5×10^{-5} M 2-mercaptoethanol, 3 μg/ml puromycin (Wako Pure Chemical Industries, Osaka, Japan), and 1% antibiotic mixture.

Cytokines, Receptors, and Antibodies—Recombinant human TNFR1 or TNFR2 Fc chimera, biotinylated anti-human TNF polyclonal antibody, and horseradish peroxidase-conjugated horseradish peroxidase were purchased from R & D Systems (Minneapolis, MN). Recombinant human or mouse TNF and IL-1β were purchased from PeproTech (Rocky Hill, NJ). The recombinant human TNF used for the *in vivo* hepatitis examination and the recombinant wtTNF-FLAG (a FLAG tag fusion protein of human TNF) were purified in our laboratory. We confirmed that the bioactivity of each TNF was equal to that of commercially available recombinant human TNF. Anti-FLAG M2 antibody was purchased from Sigma. Goat anti-human IgG antibody was purchased from Cappel (West Chester, PA). Anti-human Fas IgM was purchased from MBL (Nagoya, Japan).

Selection of Phage Displaying Structural TNF Variants (Panning)—Human TNFR1 Fc chimera was diluted to 50 μg/ml in 10 mM sodium acetate buffer, pH 4.5, and immobilized to a CM3 sensor chip using an amine coupling kit (BIAcore®, Uppsala, Sweden), which resulted in an increase of 4,000–6,000 resonance units. The phage library (1×10^{11} colony-forming units/100 μl) was injected at the flow rate of 3 μl/min over the sensor chip. After injection, the sensor chip was washed using the rinse command. Elution was carried out using 20 μl of 10 mM glycine HCl. The eluted phages were neutralized with 1 M Tris-HCl, pH 6.9. *Escherichia coli* (TG1) was infected with the eluted phages for amplification. These steps were performed twice. After the second round of selection, the phage mixture was used to infect *E. coli* and plated on LB agar/ampicillin

[3] Y. Abe, H. Shibata, K. T. Nomura, K. Minowa, H. Kamada, S. Tsunoda, Y. Tsutsumi, unpublished data.

plates. Five hundred individual colonies of *E. coli* infected with phage clones were individually picked from the LB agar plates, and each colony was grown in 2-YT medium with ampicillin (100 μg/ml) and glucose (2% w/v) at 37 °C until the A_{600} of the culture medium reached 0.4. Each culture was centrifuged; the supernatants were removed, and fresh 2-YT media with ampicillin (100 μg/ml) was added to each *E. coli* pellet. After incubation for 6 h at 37 °C, supernatants were collected and used to measure cytotoxicity in human HEp-2 cells (26, 27) and to determine the affinity for TNFR1 by ELISA (28). To measure cytotoxicity, HEp-2 cells were cultured in 96-well plates with 10% *E. coli* supernatant and 100 μg/ml cycloheximide for 18 h at 4×10^4 cells/well, and cytotoxicity was assessed by methylene blue assay as described previously (26). To determine the affinity for TNFR1 by ELISA, wells of the immune assay plates were first coated with the goat anti-human IgG antibody and then incubated with the recombinant human TNFR1 Fc chimera (0.2 μg/ml). After blocking, 2-fold diluted *E. coli* supernatant was added into each well, and the plates were incubated for 2 h at 37 °C. To each well, 200 ng/ml biotinylated anti-human TNF polyclonal antibody was added, and the plates were further incubated for 1 h at 37 °C. Wells were washed and then incubated with 1000-fold diluted avidin-horseradish peroxidase. Next, wells were washed; TMB peroxidase substrate (MOSS, Inc. Pasadena, MD) was added to each well, and the absorbance was read at 450/650 nm using a micro-plate reader.

Expression and Purification of mutTNFs—Protocol for the expression and purification of recombinant proteins was described previously (29). Briefly, mutTNFs were overexpressed in *E. coli* BL21(DE3). Expressed mutTNFs were recovered from the inclusion body, which were washed with 2.5% Triton X-100 and 0.5 M NaCl in TES buffer, and solubilized in 6 M guanidine HCl, 0.1 M Tris-HCl, pH 8.0, and 2 mM EDTA. The solubilized protein was reduced with 10 mg/ml dithioerythritol for 4 h at room temperature and then refolded by 100-fold dilution in a refolding buffer (100 mM Tris-HCl, 2 mM EDTA, 0.5 M arginine, and oxidized glutathione (551 mg/liter)). After dialyzing against 20 mM Tris-HCl, pH 7.4, containing 100 mM urea, the active trimeric proteins were purified by Q-Sepharose and Mono Q chromatography. An additional size-exclusion chromatography (Superose 12, GE Healthcare) was performed to further purify each protein. Endotoxin levels in the purified mutTNF were determined to be <300 pg/mg.

Cytotoxicity Assay—For the cytotoxicity assay, mouse L-M cells were cultured in the 96-well plates (1×10^4 cells/well) in the presence of serially diluted mouse wtTNF or mutTNFs. For the neutralization assay, cells were cultured in the presence of a constant concentration of the mouse wtTNF (5 ng/ml) and a serial dilution of the mutTNF. After incubation for 48 h, cell survival was determined by methylene blue assay as described previously (26). Jurkat cells were incubated in 96-well plates (1×10^4 cells/well) with 0.2 ng/ml anti-human Fas IgM and serially diluted R1antTNF for 24 h, and cytotoxicity was assessed using the 3-(4,5-dimethylthiazol-2-yl)-2,5-diphenyltetrazolium bromide assay.

Competitive ELISA—Inhibition of wtTNF binding to the hTNFR1 and hTNFR2 by R1antTNF was measured by ELISA as reported previously (28). The wtTNF-FLAG, a FLAG tag fusion protein of human TNF, was used as a marker protein. Briefly, the immune assay plates were coated with the goat anti-human IgG antibody and incubated with either the human TNFR1 or the human TNFR2 (0.2 μg/ml). After blocking, premixed wtTNF-FLAG (100 ng/ml) and various concentrations of R1antTNF were added to the plates. After 2 h of incubation at room temperature, the wells were washed, and the biotinylated anti-FLAG M2 antibody (0.5 μg/ml) was added to each well and then incubated for an additional period of 2 h at room temperature. Wells were washed and then incubated with the horseradish peroxidase-coupled streptavidin for 30 min at room temperature. The remaining bound wtTNF-FLAG was quantified as described above.

PC60 Assay—PC60-R1 and PC60-R2 cells were cultured at 5×10^4 cells/well with IL-1β (2 ng/ml). To evaluate the inhibitory activity, serially diluted R1antTNF and human wtTNF (200 ng/ml for PC60-R1 and 40 ng/ml for PC60-R2) were added to each cell type. After 24 h of incubation, the amount of rat GM-CSF produced was quantified by ELISA according to the manufacturer's protocol (R & D Systems).

Caspase-3/7 and NF-κB Activities—To measure the caspase-3/7 activity, the L-M cells were incubated with the human wtTNF (60 ng/ml) and R1antTNF for 8 h, and then an equal volume of the Caspase-Glo 3/7 Assay reagent (Promega Japan, Tokyo, Japan) was added to the cells. The cells were further incubated for 1 h, and luminescence was then measured using a plate reader (ALVO series, PerkinElmer Life Sciences). To measure the NF-κB activity, nuclear proteins were collected from the L-M cells stimulated with the human wtTNF (5 ng/ml) and R1antTNF for 1 h, and the activity of the NF-κB p65 in the treated cells was determined using the TransAM NF-κB p65 kit (Active Motif, Carlsbad, CA). Nuclear protein extract (1 μg) was added to an oligonucleotide-coated plate and was visualized using an anti-NF-κB p65 antibody.

RT-PCR Analysis—Total RNA was extracted from the human wtTNF and R1antTNF-stimulated HUVEC using an RNeasy mini kit (Qiagen, Valencia, CA). First-strand cDNA was synthesized from 1 μg of total RNA by using an oligo(dT_{12-18}) primer and SuperScript III reverse transcriptase (Invitrogen). Real time quantitative RT-PCR was performed using the TaqMan assay, and the PCR amplifications were carried out using an ABI 7000 thermocycler (Applied Biosystems, Foster City, CA). cDNA samples were added into a PCR master mix containing the Platinum qPCR super mix (Invitrogen) and primer/fluorescent probe sets (TaqMan Gene Expression Assays, Applied Biosystems) for the human β-actin, E-selectin, and ICAM-1 in 96-well PCR plates. Conditions for PCR were 2 min at 50 °C, 2 min at 95 °C, 45 cycles of denaturation at 95 °C for 15 s, and annealing/extension step at 60 °C for 5 s. The threshold cycle (*CT*) during the exponential phase of amplification was determined using the ABI Prism® 7000 SDS software.

Induction of Lethal Hepatitis—BALB/c mice (6-week-old females) were purchased from CLEA Japan (Tokyo, Japan). All experimental protocols for animal studies were in accordance with "Principles of Laboratory Animal Care" (National Institutes of Health) and our institutional guidelines. All reagents were prepared in pyrogen-free PBS. Control mice were injected

intravenously with 200 μl of the mixture, 100 μl of PBS, 50 μl of 20 μg/ml wtTNF, and 50 μl of 400 mg/ml GalN. Experimental mice were injected intravenously with 200 μl of the mixture, 100 μl of R1antTNF (2.7, 0.3, or 0.1 mg/ml), 50 μl of 20 μg/ml wtTNF, and 50 μl of 400 mg/ml GalN. In preliminary experiments, serum ALT levels began to increase at 6 h and were maximal 9 h after the administration of TNF/GalN. The dose used was lethal in 80–100% of mice. Blood samples were obtained from the orbital plexus under light ether anesthesia 9 h after the challenge. The serum ALT concentration was measured using a colorimetric assay kit from Wako Pure Chemical (Osaka, Japan).

Surface Plasmon Resonance Assay (BIAcore® Assay)—The binding kinetics of the wtTNF and R1antTNF were analyzed by the surface plasmon resonance (BIAcore®) technique. TNFRs were immobilized onto a CM5 sensor chip, which resulted in an increase of 3,000–3,500 resonance units. During the association phase, R1antTNF or wtTNF, diluted in running buffer (HBS-EP) at 26.1 nM, 8.7 nM or 2.9 nM, was allowed to pass over the immobilized TNFRs at a flow rate of 20 μl/min. During the dissociation phase, HBS-EP buffer was applied to the sensor chip at a flow rate of 20 μl/min. The data were analyzed globally with the BIAevaluation 3.0 software (BIAcore®) using a 1:1 binding model.

X-ray Crystallography—Purified R1antTNF was concentrated to 10 mg/ml in 20 mM Tris-HCl, pH 7.4. Initial screening using Hampton Crystal screen 1, 2 and Index kit was performed by the vapor-diffusion method with hanging drops (1 + 1 μl) at 20 °C. After optimization of crystallization conditions, orthorhombic crystals ($0.2 \times 0.2 \times 0.4$ mm^3) were obtained with 0.05 M HEPES, pH 7.5, 1.5% w/v 1,2,3-heptanetriol, and 12.5% PEG 3350. Crystals were frozen in a reservoir solution containing 20% glycerol as a cryoprotectant. X-ray diffraction data to 1.8 Å resolution were collected at the BL41XU, SPring-8 synchrotron, Harima, Japan, under flash-cooling to 100 K to reduce the effects of radiation damage. Data reduction was carried out using the DENZO and SCALEPACK. Molecular replacement was performed by using the Molrep program in ccp4i (30) using a crystal structure of the wtTNF (1TNF) (31) as a model. Cycles of manual rebuilding using O (32) and refinement using CNS (33) led to a refined structure. Final model validation was performed using the Procheck program in ccp4i (30). The model complexes of TNF-TNFR1 and R1antTNF-TNFR1 were constructed based on the crystal structure of the LT-α-TNFR1 complex (31) by using the superpose program in ccp4i.

RESULTS

Selection of TNFR1-selective mutTNF Antagonists—We previously constructed a phage library that displays structural variants of the human TNF in which random amino acid sequences replace the 6 residues (amino acids 84–89) that have been predicted to be in the TNF receptor-binding site from the crystal structure of the LT-α-TNFR1 complex (31). We confirmed that the phage library consisted of 1×10^7 independent recombinant clones. To isolate a TNFR1-selective mutant TNF (mutTNF) antagonist, the phage library was subjected to two rounds of panning against the human TNFR1 (hTNFR1) using the BIAcore® biosensor, and recovered clones were assessed for

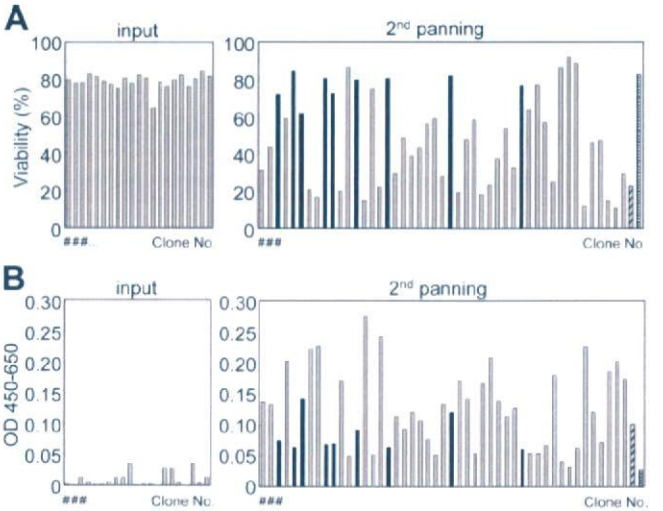

FIGURE 1. **Screening of TNFR-selective mutTNFs with no bioactivity.** Selected phage clones from the phage library were used to infect *E. coli* in a 96-well plate, and the supernatant from each infected *E. coli* was assessed to determine the bioactivity (*A*) and binding affinity (*B*) of each mutTNF. *A*, Hep-2 cells were incubated with the *E. coli* supernatant for 18 h, and cell viability was measured using the methylene blue assay. *B*, each *E. coli* supernatant was applied to the TNFR1-immobilized plate, and binding of the mutTNF to the TNFR1 was detected using the biotinylated polyclonal anti-TNF antibody. ■, mutTNF clones binding specifically to TNFR1; ▨, wtTNF; ▤, negative control.

TABLE 1

Nucleotide and amino acid sequences of 10 candidate TNFR1-selective mutTNF antagonists, which had high affinity for TNFR1 and no TNFR1 bioactivity

Clone	Position					
	Ala-84	Val-85	Ser-86	Tyr-87	Gln-88	Thr-89
T1	G(GGC)	H(CAC)	L(TCC)	Y(TAC)	T(ACG)	T(AAC)
T2	S(AGC)	T(ACC)	T(ACC)	H(CAC)	N(AAC)	Q(CAG)
T3	T(ACC)	S(AGC)	V(GTC)	Y(TAC)	P(CCC)	H(CAC)
T4	T(ACC)	N(AAC)	I(ATC)	Y(TAC)	S(AGC)	N(AAC)
T5	N(AAC)	G(GGC)	A(GCG)	Y(TAC)	E(GAG)	T(ACG)
T6	G(GGC)	G(GGC)	P(CCG)	Y(TAC)	Q(CAG)	R(CGG)
T7	S(AGC)	P(CCG)	R(AGG)	V(GTC)	S(TCC)	G(GGC)
T8	T(ACC)	P(CCC)	A(GCC)	I(ATC)	N(AAC)	R(CGG)
T9	A(GCG)	P(CCC)	G(GGC)	Y(TAC)	S(TCC)	H(CAC)
T10	S(TCC)	P(CCC)	Q(CAG)	Y(TAC)	S(AGC)	V(GTC)

TNFR1-mediated cytotoxicity and affinity for TNFR1. Although the number of phage clones that had strong cytotoxicity increased after the second panning, phage clones having almost no cytotoxicity but significant affinity for TNFR1 were also recognized (Fig. 1). Eventually, we identified 10 mutTNF candidates as the TNFR1-selective antagonists (Table 1), and we further investigated the properties of these 10 potential antagonists. All 10 mutTNFs were recombinantly expressed in *E. coli*, out of which we could only purify nine mutTNFs (T1–T4, T6–T10); for some unknown reason, we were unable to purify the mutTNF-T5. All nine purified mutTNFs displayed a molecular mass of 17 kDa by gel electrophoresis and gel filtration analyses and formed homotrimeric complexes in the same manner as the wtTNF (data not shown). We measured the bioactivities and antagonistic activities of nine mutTNFs on the mouse TNFR1 (mTNFR1) using the L-M cells, a cell line derived from the L929 cells, and the results are shown in Fig. 2. The mutTNF-T2 showed the lowest biological activity even when tested at high concentrations (Fig. 2*A*). Both mutTNF-T2 and mutTNF-T7 inhibited the wtTNF-induced cytotoxicity

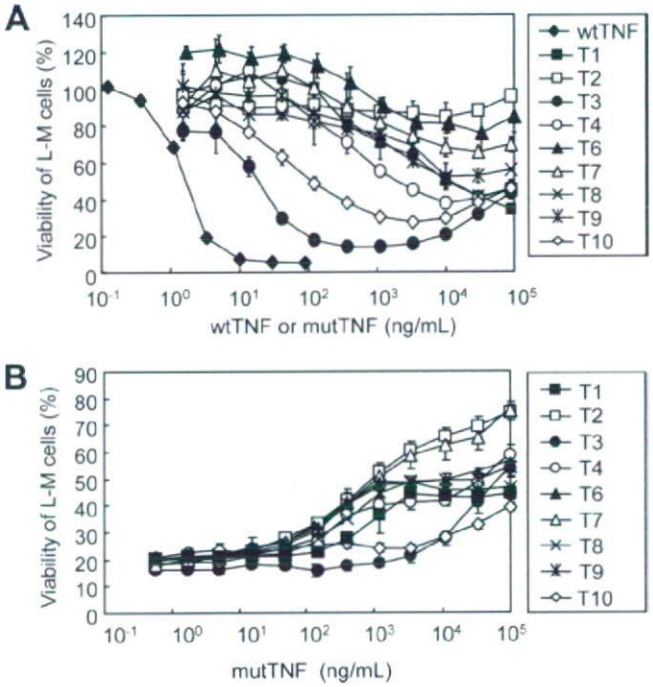

FIGURE 2. **Bioactivities and antagonistic activities of candidate TNFR1-selective mutTNFs.** *A*, diluted mutTNFs were added to the L-M cells and incubated for 48 h at 37 °C. After incubation, cell viability was measured using the methylene blue assay. *B*, indicated dilutions of a given mutTNF and a constant concentration of mouse TNF (5 ng/ml) were mixed and added to the L-M cells. Cell viability was measured as described above, and the antagonistic activity was assessed as described under "Experimental Procedures." Each data point represents the mean ± S.D.

TABLE 2

Dissociation constants of the mutTNFs determined from the SPR analysis of the interactions between the mutTNFs and the hTNFR1 or hTNFR2

Clone	TNFR1 K_D	TNFR2 K_D	TNFR1 selectivity
	nM	nM	
wtTNF	1.4	2.1	1.0
T1	5.0	28.1	3.7
T2	3.5	92,900.0	17,677.4
T3	1.2	4.6	2.6
T4	5.0	26.9	3.5
T6	7.6	2.3	0.2
T7	2.3	12.9	3.7
T8	2.6	1230.0	308.8
T9	6.8	8.4	0.8
T10	5.1	8.8	1.1

most efficiently (Fig. 2*B*). Additionally, the TNF receptor selectivity of the nine mutants was measured using the BIAcore® biosensor technique. Both mutTNF-T2 and mutTNF-T8 showed superior TNFR1 selectivity as compared with the other mutants (Table 2). Based on these results, mutTNF-T2 was chosen for further analysis and renamed as R1antTNF; this mutant displayed the highest selectivity for TNFR1 binding and possessed the lowest biological activity and highest antagonistic activity on mTNFR1.

Inhibition of TNFR1-mediated Intracellular Signaling and Expression of Adhesion Molecule by R1antTNF—Activation of TNFR1 by TNF leads to the recruitment of the adaptor protein TRADD to its cytoplasmic death domain and induction of apoptosis because of the activation of caspase-8/10 and caspase-3/7 (34). If R1antTNF inhibited the wtTNF-mediated cytotoxicity

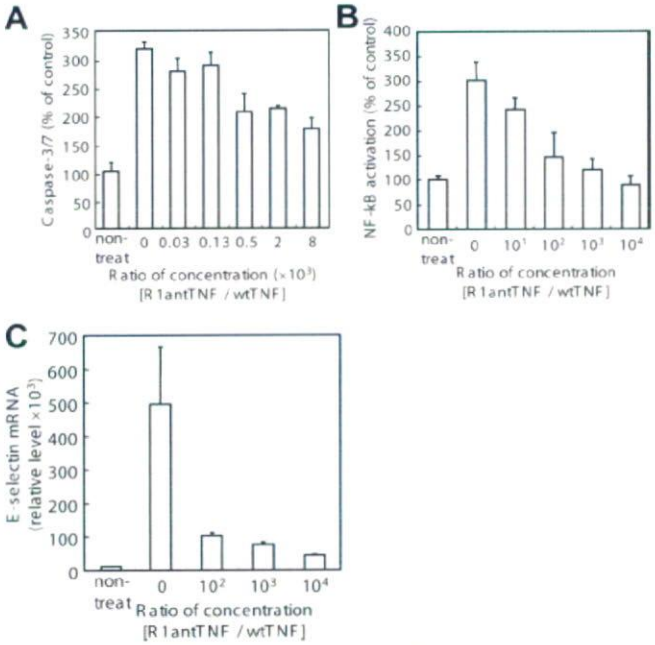

FIGURE 3. **R1antTNF-mediated inhibition of signal transduction and expression of adhesion molecule.** Activation of caspase-3/7 (*A*) and NF-κB (*B*) induced by the human wtTNF (60 and 5 ng/ml, respectively) in L-M cells was measured as described under "Experimental Procedures." Incubation times for the caspase-3/7 was 8 h and that for the NF-κB was 1 h. *C*, to measure the E-selectin expression, indicated amounts of R1antTNF were mixed with the human wtTNF (10 ng/ml), and the mixture was added to the HUVEC and incubated for 3 h. Total RNAs were prepared from these cells and were used for the RT-PCR analysis. Each data point represents the mean ± S.D.

in L-M cells by blocking the binding of wtTNF to TNFR1, R1antTNF could also inhibit this activation of caspase cascade. Thus, we investigated the inhibitory activity of R1antTNF on the wtTNF-induced activation of caspase-3/7. Indeed R1antTNF significantly inhibited the caspase-3/7 activation induced by the wtTNF in L-M cells in a dose-dependent manner (Fig. 3*A*). TNFR1 signaling also activates the transcription factor NF-κB, leading to the activation of inflammatory and anti-apoptotic genes (34). We found that the wtTNF-mediated NF-κB activation in mouse L-M cells was completely blocked by the addition of R1antTNF (Fig. 3*B*). NF-κB activated by the TNF/TNFR1 interaction regulates several cell adhesion molecules in the endothelial cells, such as E-selectin, ICAM-1, and VCAM-1 (35). Therefore, we assessed the inhibitory activity of R1antTNF on the wtTNF-induced expression of cell adhesion molecules in HUVEC cells. We found that the R1antTNF suppressed the expression of the E-selectin gene (Fig. 3*C*). These results suggested that R1antTNF inhibited the function of wtTNF by blocking the wtTNF-induced signal transduction.

TNFR1-selective Antagonistic Activity of R1antTNF—To determine the potency of the TNFR1-selective antagonistic activity, we used competitive ELISA to investigate whether the R1antTNF would inhibit only the binding of the wtTNF to hTNFR1. R1antTNF inhibited the binding of wtTNF to hTNFR1 in a dose-dependent manner just like the wtTNF did, but it did not affect the binding of wtTNF to hTNFR2 (Fig. 4, *A* and *B*). This result correlates to the results obtained using the BIAcore technique. To confirm that this antagonistic activity of R1antTNF was receptor-selective, a competitive bioassay was

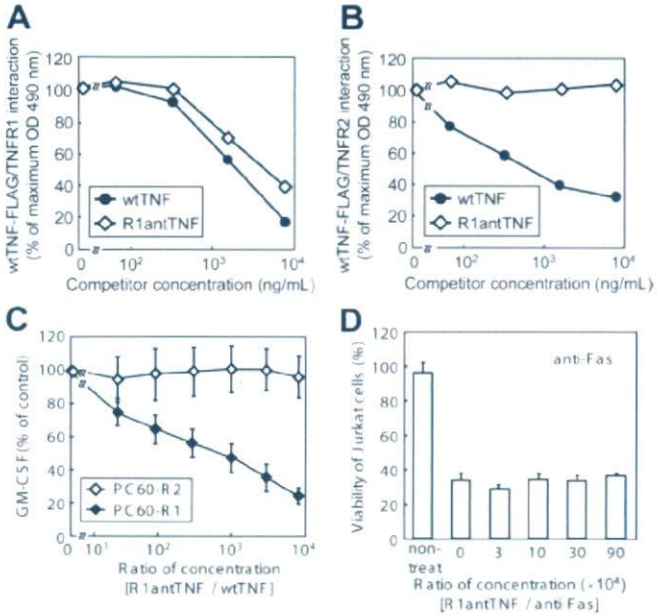

FIGURE 4. **TNFR1-selective antagonistic properties of R1antTNF.** Different concentrations of wtTNF and R1antTNF were premixed with a fixed concentration of wtTNF-FLAG and were added to the hTNFR1-coated (*A*) or hTNFR2-coated plates (*B*). Binding of wtTNF-FLAG was determined as described under "Experimental Procedures." *C*, to determine the receptor-type contribution to bioactivity, serially diluted R1antTNF was mixed with the human wtTNF (PC60-R1, 200 ng/ml; PC60-R2, 40 ng/ml), and added to the PC60-Rs cells. After 24 h, production of the rat GM-CSF was measured by ELISA as described under "Experimental Procedures." ◆, PC60-R1; 224 , PC60-R2. *D*, Jurkat cells were incubated with the anti-human Fas IgM (0.2 ng/ml) and indicated dilutions of R1antTNF for 24 h, and cytotoxicity was assessed using the 3-(4,5-dimethylthiazol-2-yl)-2,5-diphenyltetrazolium bromide assay.

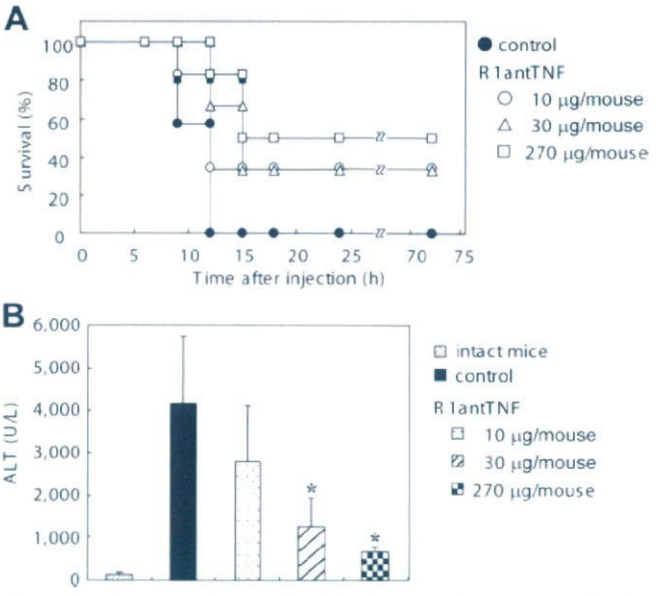

FIGURE 5. **Therapeutic effect of R1antTNF in lethal hepatitis model.** Mice were injected intravenously with recombinant human TNF (1.0 μg)/GalN (20 mg) and R1antTNF or PBS. *A*, survival rates of the mice in the TNF/GalN-induced hepatitis model were measured over a period of 72 h ($n = 6$). *B*, blood samples were collected 9 h after the challenge. Serum concentration of alanine aminotransferase (*ALT*) was measured as described under "Experimental Procedures" ($n = 6$). Data represent the mean ± S.E. Statistical significance *versus* control mice was calculated by unpaired Student's *t* test (*, $p < 0.05$).

performed using PC60-R1 and PC60-R2 cell lines that stably expressed hTNFR1 and hTNFR2 (25), respectively. R1antTNF efficiently inhibited the wtTNF-induced GM-CSF production in the PC60-R1 cells but not in the PC60-R2 cells (Fig. 4*C*), confirming the TNFR1-specific antagonistic activity. The risk of cross-activity to other TNF receptor superfamily members was assessed by Fas-induced cytotoxicity assay on Jurkat cell (Fig. 4*D*). R1antTNF did not affect the Fas-mediated signaling, which suggest that R1antTNF was highly selective proteo-antagonist of TNFR1. These data suggest that the R1antTNF not only binds to the TNFR1 selectively but also has TNFR1-selective inhibitory activity.

Therapeutic Efficacy of R1antTNF on Lethal Hepatitis Model—To assess the inhibitory activity and therapeutic effect of R1antTNF *in vivo*, we investigated the protective effect of R1antTNF in the TNF/D-(+)-galactosamine (GalN)-induced hepatitis model. GalN is a hepatotoxin that inhibits transcription and translation in hepatocytes. The combined administration of GalN and TNF causes massive apoptosis of hepatocytes and induces lethal hepatitis (36). In the control group, all mice died within 12 h after a lethal challenge with TNF/GalN (Fig. 5*A*). Co-treatment with R1antTNF improved the survival rate. Especially, in mice co-treated with R1antTNF (270 μg/mouse), the survival rates were 5/6 after 12 h and 3/6 after 24 h (Fig. 5*A*). The surviving mice were still alive several weeks after the treatment. In the control group, the serum levels of ALT, a marker for liver damage, were markedly elevated. In contrast, co-treatment of mice with R1antTNF suppressed the elevation of ALT levels in a dose-dependent manner (Fig. 5*B*). These results demonstrated that R1antTNF had antagonistic activity not only *in vitro* but also *in vivo*, and exhibited remarkable inhibitory effect on hepatitis.

TABLE 3
Binding properties of R1antTNF

Receptor	Kinetic parameter	wtTNF	R1antTNF
hTNFR1	k_{on} ($\times 10^5$ $M^{-1}s^{-1}$)[a]	3.6 ± 2.9	8.3 ± 0.1
	k_{off} ($\times 10^{-4}$ s^{-1})[b]	5.0 ± 1.3	28.7 ± 5.9
	K_D ($\times 10^{-9}$ M)[c]	1.4 ± 2.7	3.5 ± 1.8
hTNFR2	k_{on} ($\times 10^5$ $M^{-1}s^{-1}$)	7.0 ± 3.2	0.000001 ± 0.0
	k_{off} ($\times 10^{-4}$ s^{-1})	14.5 ± 4.9	0.1 ± 0.0
	K_D ($\times 10^{-9}$ M)	2.1 ± 1.1	92,900 ± 96.1
mTNFR1	k_{on} ($\times 10^5$ $M^{-1}s^{-1}$)	2.5 ± 0.0	18.7 ± 0.2
	k_{off} ($\times 10^{-4}$ s^{-1})	1.9 ± 0.3	96.6 ± 0.8
	K_D ($\times 10^{-9}$ M)	0.8 ± 0.4	5.2 ± 0.5

[a] k_{on} is the association kinetic constant.
[b] k_{off} is the dissociation kinetic constant.
[c] K_D is the equilibrium dissociation constant. Kinetic parameters for each TNF was calculated from the respective sensorgram by BIAevaluation 3.0 software.

Binding Mode and Affinity of R1antTNF—The dissociation constant (K_d) of R1antTNF binding to hTNFR1 was very similar to that of the wtTNF (Table 2), whereas the R1antTNF (mutTNF-T2) has no bioactivity through TNFR1 (Fig. 2*A*). We predicted that the binding modes of the wtTNF and R1antTNF to the TNFR1 are different, resulting in different biological activities. To quantify the altered binding mode of R1antTNF, we examined the binding kinetics of the R1antTNF for the mTNFR1, hTNFR1, and hTNFR2 using the surface plasmon resonance technique (Table 3). Indeed, the dissociation kinetic constants (k_{off}) of the R1antTNF for the human and mouse